Semiclassical sum rules for matrix elements and response functions in chaotic and in integrable quantum billiards

B. Mehlig
Theoretical Physics, University of Oxford, 1 Keble Road, Oxford OX1 3NP, Great Britain
(Received 18 December 1997; revised manuscript received 12 August 1998)

It is shown that expectation values and transition matrix elements in classically chaotic quantum systems may not fluctuate randomly, since features of the short-time classical dynamics significantly affect the fluctuations. We analyze semiclassical sum rules constraining expectation values and transition matrix elements in classically chaotic and integrable quantum systems. We show that these sum rules exhibit a wealth of interesting structures (resonances and oscillatory contributions) as well as interesting properties, such as their asymptotic decay. It is shown how these properties can be explained semiclassically, in terms of periodic and quasiperiodic classical motion. In particular, we analyze how phase-space inhomogeneities in chaotic systems give rise to localization of wave functions and hence to exceptionally large matrix elements. These are related to resonances in classical autocorrelation functions. As an example, we consider a family of billiards in two dimensions the classical dynamics of which ranges from integrable to chaotic. [S1063-651X(99)06201-7]

PACS number(s): 05.45.Mt

I. INTRODUCTION

Spectral properties of classically chaotic quantum systems have received considerable attention over the last years, and it is now well established that spectral fluctuations in such systems on small energy scales are universal. Furthermore, it has been shown that spectral correlations on larger energy scales can be qualitatively and quantitatively understood from a semiclassical point of view [1,2]. It is clearly highly desirable to reach a similarly thorough understanding of the statistical properties of expectation values and transition matrix elements since they describe the influence of time-independent and time-dependent perturbations and thus many experimental situations.

In weakly disordered quantum systems, the fluctuations of diagonal and nondiagonal matrix elements are Gaussian and described by random matrix theory [3,4]. While the average of nondiagonal matrix elements vanishes in the semiclassical regime, diagonal matrix elements are not necessarily distributed around zero. A semiclassical estimate for the mean is given by the phase-space average of the observable in question. The variances of diagonal and nondiagonal matrix elements are related [5], and hence fluctuations of expectation values and transition matrix elements in such systems are exhaustively characterized by the mean and the variance of the distribution of diagonal matrix elements.

One might expect that this would equally apply to diagonal and nondiagonal matrix elements in classically chaotic quantum systems. It has indeed been shown that fluctuations of expectation values in systems with exponentially decaying classical correlations are described by random matrix theory [6]. Recently, fluctuations of expectation values in chaotic systems have attracted considerable attention [5–14].

In many chaotic systems, however, and this includes most of the experimentally accessible systems, classical dynamics exhibits structures on small time scales, leading to nonexponential decay of correlations. In this case random matrix theory does not apply and fluctuations of diagonal and nondiagonal quantum-mechanical matrix elements can differ substantially from the predictions of random matrix theory. Consider, for example, Fig. 1(a), which shows the histogram of nearest-neighbor level spacings for a chaotic (and largely ergodic) quantum billiard. The distribution is well approximated by Wigner's surmise, the prediction of random matrix theory. Figure 1(b), on the other hand, shows a histogram of expectation values of the dipole operator in the same system. The distribution is far from Gaussian.

In this paper we analyze fluctuations of diagonal and nondiagonal matrix elements in a family of quantum billiards, exhibiting integrable and chaotic classical dynamics. We show how structures in the classical short-time dynamics influence quantum-mechanical matrix elements. We analyze semiclassical sum rules constraining the fluctuations of diagonal and non-diagonal matrix elements [5,15–17] and explain in detail how phase-space structures influence matrix elements in integrable and chaotic quantum systems.

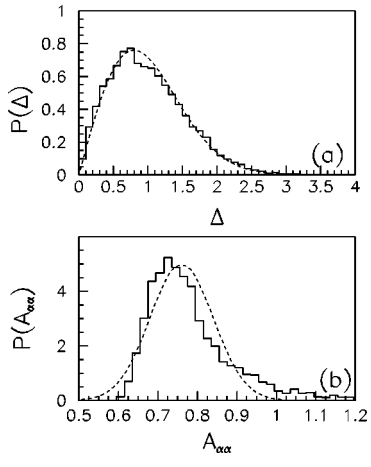

FIG. 1. (a) Histogram of the nearest-neighbor level spacings for a chaotic quantum billiard. Wigner's surmise $P(\Delta) = \Delta\pi/2 \exp(-\pi\Delta^2/4)$ is also shown (dashed line). (b) The histogram of expectation values of the operator $\boldsymbol{r}^2$ in the same system shows strong non-Gaussian behavior.

The lowest order classical contributions to the sum rules in chaotic systems have previously been considered: Austin and Wilkinson [18,19] have studied the quartic oscillator and a hyperbolic billiard. Prosen and Robnik have performed quantum calculations for a range of chaotic billiards [20,21]. Boosé *et al.* have studied the hydrogen atom in a strong magnetic field [22].

The leading order semiclassical contributions to sum rules for matrix elements in integrable and chaotic systems were analyzed in [23,24]. In the present article, the calculations reported in [23,24] will be discussed in detail. In addition, the corresponding sum rules for diagonal and nondiagonal matrix elements in integrable systems will be derived.

As has been outlined above, a classical and semiclassical analysis of diagonal and nondiagonal matrix elements is interesting from a theoretical point of view in its own right. However, a semiclassical theory of matrix elements is also of interest in view of recent experiments on clean $Ga_xAl_{1-x}As$ heterostructures. In many respects, these systems behave essentially classically. In order to explain various features of quantum magnetoconductivity in an array of antidots, for instance, purely classical models (incorporating the essential structure of classical phase space) are sufficient [25]. We derive the relevant classical approximations to quantum response functions and compare them in detail with fully quantum-mechanical calculations. Apart from providing a quantitative theory for the magnetoconductivity in antidot arrays — as discussed in Refs. [25,26] — these results can be applied to describe the absorption of radiation and the polarizability of small conducting particles in the ballistic [27,28] but also in the diffusive regime [29].

In some cases it may be necessary to complement the theory based on purely classical phase space information by a semiclassical calculation. More refined measurements of the magnetoconductivity [30] have shown characteristic oscillations. They are thought to arise semiclassically from periodic orbit contributions of the type discussed in the present article [31,32]. A comparison of such semiclassical contributions with accurate quantum calculations was first published in [24] and [23]. In the present paper we give a detailed account of these calculations and discuss the relevance to the above-mentioned experiments.

Finally, a semiclassical theory for diagonal matrix elements may be used to calculate the thermodynamic response of a system of noninteracting particles (such as electrons in a ballistic cavity) to static external perturbations.

The present article is organized as follows. In Sec. II we briefly describe the system used for the quantum-mechanical calculations, a parametric family of quantum billiards [33,34,20,35]. In Sec. III we outline the semiclassical theory used in the present paper. Section IV describes the results for densities of diagonal matrix elements, in integrable as well as in chaotic systems. In Sec. V we discuss densities of nondiagonal matrix elements. In Sec. VI we discuss the response of quantum billiards to external perturbations, using the results of Secs. III–V. Finally, in Sec. VII we summarize and draw conclusions.

II. ROBNIK'S BILLIARD

In this section we briefly describe the system used in the following to illustrate our results. It is a family of two-dimensional quantum billiards, first studied by Robnik [33,34], Prosen and Robnik [20], and Prosen [21,35] and others. A review of the classical and quantum properties of this system can be found in Refs. [33,34]. In the following we restrict ourselves to introducing those features of the system necessary to make the ensuing discussion in Secs. IV–VI intelligible.

The boundary of Robnik's billiard is parametrized by $r=1+a\cos\phi$ in polar coordinates (r,ϕ). For $a=0$, the boundary is just a circle. Motion in the circular billiard is regular. As the domain is deformed, classical motion ceases to be integrable and soft chaos according to the KAM-Lazutkin theorem develops. The last large islands of stability disappear just before $a=1/2$. For $a=1$, the system has been proven to be ergodic. In the following sections, we discuss two cases, the integrable limit $(a=0)$ and the largely ergodic case $(a=1/2)$. We take the mass $m=1/2$.

The integrable limit. For $a=0$, classical motion in phase space is integrable. A possible choice of action variables has been given in [36]: since angular momentum $L_z=\dot{\phi}r^2$ is conserved, one may take

$$I_1=\dot{\phi}\,r^2=r_{\min}\sqrt{E}\,, \tag{1}$$

where $r_{\min}$ is the minimal value of the radius at the turning point of the radial motion. The second action variable is taken to be

$$I_2=\frac{1}{\pi}\int_{r_{\min}}^{1}dr\ \sqrt{E-\frac{I_1^2}{r^2}}. \tag{2}$$

The corresponding angle variables are

$$\theta_1=\begin{cases}\phi-\arccos\left(\dfrac{r_{\min}}{r}\right)+\dfrac{\omega_1}{2\sqrt{E}}\sqrt{r^2-r_{\min}^2}, & \text{for } 0<t<\dfrac{T_2}{2},\\[2ex] \phi+\arccos\left(\dfrac{r_{\min}}{r}\right)-\dfrac{\omega_1}{2\sqrt{E}}\sqrt{r^2-r_{\min}^2}, & \text{for } \dfrac{T_2}{2}<t<T_2,\end{cases} \tag{3}$$

$$\theta_2=\omega_2\,t\,, \tag{4}$$

TABLE I. Properties of the shortest unstable periodic orbits for $a=1/2$ and positive parity π^+. L_p denotes the length, λ_p the Lyapunov exponent, μ_p the Maslov exponent, $w_{pr}=L_p/\sqrt{|\det(M_p^r-1)|}$ the semiclassical amplitude and x_p the average of the observable $A=x$ around the periodic orbit p.

PO	$L_p/2\pi$	λ_p	μ_p	type	$w_{pr}/2\pi$ $\times\exp(-i\pi\mu_p/2)$	x_p
2^1 $(r=\frac{1}{2})$	0.3504	0.6165	3	ih	$-i0.1672$	0.433
	0.7009		6	h	-0.2670	
$2,\pi^+$	0.6366	1.5907	5	ih	$i0.2998$	0.500
	1.2732		10	h	-0.1299	
3	0.8601	2.2364	8	ih	0.2540	0.463
3^1	0.8924	1.7220	9	h	$i0.4594$	0.467
	1.7848		18	h	-0.1648	
4	0.9479	2.6561	11	ih	$-i0.2347$	0.463
4^1	0.9649	2.0947	12	h	0.3861	0.471
8^4 $(r=\frac{1}{2})$	1.2899	2.8308	11	h	$-i0.3303$	0.495
8^5 $(r=\frac{1}{2})$	1.3052	1.9470	12	ih	0.4315	0.493
5^2	1.6003	3.5563	14	ih	-0.2629	0.462
5^3	1.6251	2.8679	15	h	$-i0.4107$	0.463
6^{2a}	1.7330	2.9845	17	ih	$i0.3710$	0.467
6^2	1.7343	2.4970	18	h	-0.5423	0.469
7^2	1.8497	4.4276	20	ih	0.1998	0.467
7^3	1.8640	3.7346	21	h	$i0.2951$	0.469

where t is the time along the trajectory, $\boldsymbol{\omega}=(\omega_1,\omega_2)$ are the angular and radial frequencies and T_1 and T_2 are the corresponding periods.

The largely ergodic case. For $a=1/2$, motion is largely ergodic and all large islands of stability have disappeared. While it has been shown in Ref. [37] that isolated stable orbits persist at $a=1/2$ and beyond, it is safe to ignore these small islands for our purposes and we will assume that the relevant periodic orbits of the system are isolated. Table I summarizes the properties of the shortest unstable periodic orbits of the billiard at $a=1/2$. See also Fig. 2. The orbits are labeled by the number of hits at the boundary. The families of whispering gallery orbits, which originate from tori with winding number $1/n$ $(2/n)$ are denoted by n and n^1 $(n^2$ and $n^3)$. The asymmetric six-hit orbit, which bifurcates from 6^2 at $a\approx 0.44$, is denoted by 6^{2a}. Since the length of both orbits is still very close at $a=1/2$, their contribution to the Fourier transform of the quantum spectra cannot be resolved.

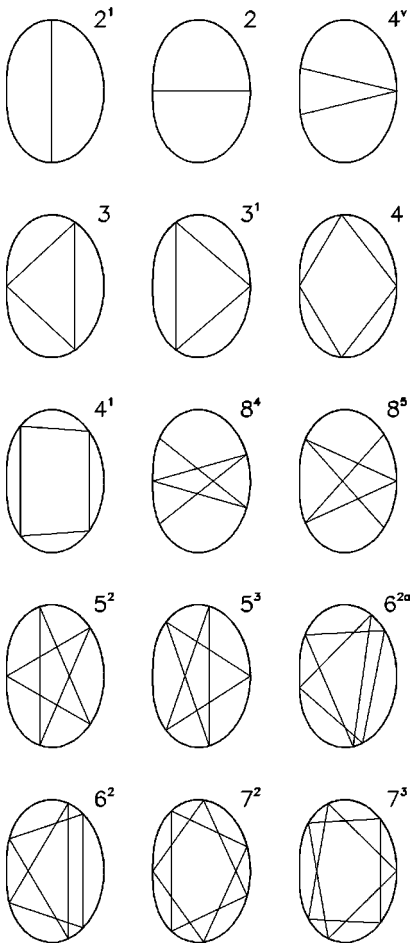

FIG. 2. Isolated periodic orbits for Robnik's billiard with $a=1/2$, as listed in Table I.

III. SEMICLASSICAL THEORY FOR MATRIX ELEMENTS

In this section we discuss the semiclassical theory for local averages of matrix elements of the form

$$d_A(E)=\sum_\alpha \langle\psi_\alpha|\hat{A}|\psi_\alpha\rangle\,\delta(E-E_\alpha)\,, \tag{5}$$

$$C(E,\hbar\omega)=\sum_{\alpha\beta} |\langle\psi_\alpha|\hat{A}|\psi_\beta\rangle|^2\,\delta(\hbar\omega+E_\alpha-E_\beta)\,\delta(E-E_\alpha)\,. \tag{6}$$

Here E_α and $|\psi_\alpha\rangle$ are the eigenvalues and eigenstates of the Hamiltonian $\hat{H}$. Semiclassical approximations for these local densities provide sum rules for matrix elements constraining their fluctuation properties. The semiclassical evaluation of Eqs. (5) and (6) closely follows Gutzwiller's semiclassical approximation for the density of states,

$$d(E)=\sum_\alpha \delta(E-E_\alpha)\,. \tag{7}$$

Semiclassically, $d(E)$ is obtained as a sum of two terms,

$$d(E)=\langle d(E)\rangle+\tilde{d}(E)\,. \tag{8}$$

Here $\langle d(E)\rangle$ is the so-called Weyl contribution. It is a smooth function of the energy E and asymptotically $\langle d(E)\rangle$ is energy independent for two-dimensional quantum billiards. The second term $\tilde{d}(E)$ is an oscillatory contribution to the density of states that can be expressed as a sum over periodic orbits.

Similarly, the energy dependence of the densities (5) and (6) can be split into smooth and oscillatory parts. The smooth part is again related to zero-length orbits, and the oscillatory contributions can be expressed as sums of periodic orbits. In the following we treat classically chaotic as well as inte-

grable systems. Section III A deals with the chaotic case while Sec. III B deals with the integrable case.

A. Classically chaotic systems

In this section we derive semiclassical approximations for the local densities defined in Eqs. (5) and (6) for chaotic systems. The results derived in this section are originally due to Wilkinson [16,5]. In Ref. [17], Wilkinson's derivation was reformulated for the case of diagonal matrix elements using Wigner transforms. Along similar lines, a semiclassical expression for Eq. (6) may be obtained, as will be seen in the following. It is convenient to rewrite Eqs. (5) and (6) as follows:

$$d_A(E)=\mathrm{Tr}[\hat{A}\,\delta(E-\hat{H})], \tag{9}$$

$$C(E,\hbar\omega)=\frac{1}{2\pi\hbar}\int dt\,\exp(i\omega t)\,\mathrm{Tr}[\hat{A}_t\hat{A}\,\delta(E-\hat{H})], \tag{10}$$

where $\hat{A}_t=\exp(-i\hat{H}t/\hbar)\,\hat{A}\exp(i\hat{H}t/\hbar)$. The δ functions are expressed in terms of retarded and advanced Green's functions,

$$\delta(E-\hat{H})=-\frac{1}{2\pi i}[\hat{G}^{+}(E)-\hat{G}^{-}(E)]\,. \tag{11}$$

The next step is to rewrite the traces in Eqs. (9) and (10) as phase space integrals, e.g.,

$$\mathrm{Tr}[\hat{A}_t\hat{A}\,\hat{G}^{\pm}(E)]=\int\frac{d\boldsymbol{p}\,d\boldsymbol{r}}{(2\pi\hbar)^d}G^{\pm}_{\mathrm{W}}(\boldsymbol{p},\boldsymbol{r};E)\,(A_tA)_{\mathrm{W}}(\boldsymbol{p},\boldsymbol{r}), \tag{12}$$

where $G^{\pm}_{\mathrm{W}}(\boldsymbol{p},\boldsymbol{r};E)$ is the Wigner transform of the Green's function $G^{\pm}(\boldsymbol{r}',\boldsymbol{r};E)$

$$G^{\pm}_{\mathrm{W}}(\boldsymbol{p},\boldsymbol{r};E)=\int d\boldsymbol{r}_1\,G^{\pm}(\boldsymbol{r}+\boldsymbol{r}_1/2,\boldsymbol{r}-\boldsymbol{r}_1/2;E)\exp\left(-\frac{i}{\hbar}\boldsymbol{p}\cdot\boldsymbol{r}\right) \tag{13}$$

and $(A_tA)_{\mathrm{W}}(\boldsymbol{p},\boldsymbol{r})$ is the Wigner transform of $\hat{A}_t\hat{A}$. To lowest order in $\hbar$ one has

$$(A_tA)_{\mathrm{W}}(\boldsymbol{p},\boldsymbol{r})=A(\boldsymbol{p}_t,\boldsymbol{r}_t)A(\boldsymbol{p},\boldsymbol{r})+\frac{\hbar}{2i}\{A(\boldsymbol{p}_t,\boldsymbol{r}_t),A(\boldsymbol{p},\boldsymbol{r})\}+O(\hbar^2), \tag{14}$$

where $\{,\}$ is the Poisson bracket. In the following only the lowest-order contributions in $\hbar$ to $\langle C(E,\hbar\omega)\rangle$ and $\tilde{C}(E,\hbar\omega)$ will be considered. A semiclassical approximation to $G^{\pm}_{\mathrm{W}}(\boldsymbol{p},\boldsymbol{r};E)$ is obtained by expressing the Green's function in terms of the propagator,

$$G^{+}(\boldsymbol{r}'',\boldsymbol{r}';E)=\frac{1}{i\hbar}\int_0^\infty dt\,K(\boldsymbol{r}'',\boldsymbol{r}';t)\exp\left(\frac{i}{\hbar}Et\right). \tag{15}$$

For K we substitute the Van Vleck propagator,

$$K(\boldsymbol{r}'',\boldsymbol{r}';t)=\left(\frac{1}{2\pi i\hbar}\right)^{d/2}\sum_{\substack{\text{classical}\\ \text{paths}}}\left|\det\left(-\frac{\partial^2R}{\partial\boldsymbol{r}''\partial\boldsymbol{r}'}\right)\right|^{1/2}\times\exp\left[\frac{i}{\hbar}R(\boldsymbol{r}'',\boldsymbol{r}';t)-i\frac{\pi}{2}\kappa\right], \tag{16}$$

where $R(\boldsymbol{r}'',\boldsymbol{r}';t)$ is the action integral. It will be seen in the following that the two contributions to $C(E,\hbar\omega)$, namely the smooth part $\langle C(E,\hbar\omega)\rangle$ and the oscillatory part $\tilde{C}(E,\hbar\omega)$ are obtained by two different approximations to the Van Vleck propagator, the short-time approximation and the stationary-phase approximation for the time integral.

1. Short-time approximation

The short-time approximation to $K(\boldsymbol{r}'',\boldsymbol{r}';t)$ yields the smooth contributions to $C(E,\hbar\omega)$. For short times, $R(\boldsymbol{r}'',\boldsymbol{r}';t)\simeq m(\boldsymbol{r}''-\boldsymbol{r}')/4t-tV(\boldsymbol{r}''+\boldsymbol{r}')/2$. Substituting this into Eq. (13) and performing the integral over $\boldsymbol{r}_1$ in stationary phase approximation, one obtains

$$G^{+}_{\mathrm{W}}(\boldsymbol{p},\boldsymbol{r};E)=\frac{1}{E-H(\boldsymbol{p},\boldsymbol{r})+i0^{+}}. \tag{17}$$

Using Eqs. (10) and (12) one finds in $d=2$ dimensions

$$\begin{aligned}\langle C(E,\hbar\omega)\rangle&\simeq\frac{1}{2\pi\hbar}\int_{-\infty}^{\infty}dt\,\exp(i\omega t)\int\frac{d\boldsymbol{p}\,d\boldsymbol{r}}{(2\pi\hbar)^2}\\&\quad\times\delta[E-H(\boldsymbol{p},\boldsymbol{r})]\,A(\boldsymbol{p}_t,\boldsymbol{r}_t)\,A(\boldsymbol{p},\boldsymbol{r})\\&\equiv\frac{1}{2\pi\hbar}\int_{-\infty}^{\infty}dt\,\exp(i\omega t)\,\langle A(\boldsymbol{p}_t,\boldsymbol{r}_t)\,A(\boldsymbol{p},\boldsymbol{r})\rangle\,,\end{aligned} \tag{18}$$

where $\langle\,\rangle$ denotes an average over the energy shell. Equation (18) gives the leading order classical contribution to the smooth part of $C(E,\hbar\omega)$. For an ergodic system, the phase-space average can be expressed in terms of a classical autocorrelation function along an ergodic trajectory

$$\langle A(\boldsymbol{p}_t,\boldsymbol{r}_t)\,A(\boldsymbol{p},\boldsymbol{r})\rangle=\langle d(E)\rangle\,C^{\mathrm{cl}}(E,t), \tag{19}$$

where $C^{\mathrm{cl}}(E,t)$ is given by

$$C^{\mathrm{cl}}(E,t)=\lim_{T\to\infty}\frac{1}{T}\int_0^T dt'\,A(\boldsymbol{p}_{t+t'},\boldsymbol{r}_{t+t'})\,A(\boldsymbol{p}_{t'},\boldsymbol{r}_{t'})\,. \tag{20}$$

The analogous expression for the density (5) is

$$\begin{aligned}\langle d_A(E)\rangle&\simeq\int\frac{d\boldsymbol{p}\,d\boldsymbol{r}}{(2\pi\hbar)^2}\,\delta[E-H(\boldsymbol{p},\boldsymbol{r})]\,A(\boldsymbol{p},\boldsymbol{r})\\&\equiv\langle d(E)\rangle\,\langle A(\boldsymbol{p},\boldsymbol{r})\rangle_{\mathrm{mc}}\end{aligned} \tag{21}$$

as derived in Refs. [16] and [17]. The second equality defines the microcanonical phase-space average of A. It should be emphasized that Eqs. (18) and (21) give only the leading

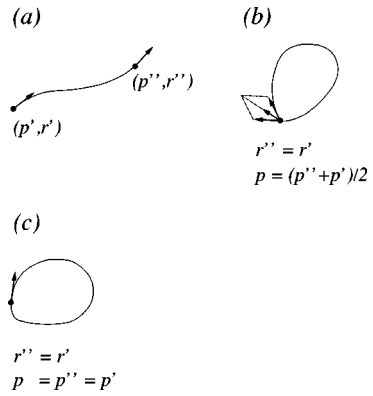

FIG. 3. Illustrating the contributions to Eqs. (23), (24), and (25). (a) shows a path from $\boldsymbol{r}'$ to $\boldsymbol{r}''$, with intial momentum $\boldsymbol{p}'$ and final momentum $\boldsymbol{p}''$. (b) shows a closed path returning to $\boldsymbol{r}'$, with different initial and final momenta $\boldsymbol{p}'$ and $\boldsymbol{p}''$, with $\boldsymbol{p}=(\boldsymbol{p}'+\boldsymbol{p}'')/2$. (c) shows a periodic orbit with $\boldsymbol{p}=\boldsymbol{p}'=\boldsymbol{p}''$.

order contribution to the smooth parts of the densities (5) and (6). Higher corrections to Eq. (21) are considered in Sec. IV A .

2. Oscillatory contributions

In order to calculate the oscillatory contributions to Eqs. (5) and (6), the integral in Eq. (15) is performed in the stationary phase approximation, using the Van Vleck propagator. This calculation is outlined in the present section. It will be assumed that all periodic orbits of the classical system are isolated. Hence the following derivation is inadequate in the case of classically integrable systems, where motion on tori is degenerate. These systems will be dealt with separately.

It is well known that approximating the time integral in Eq. (15) within the stationary-phase approximation yields an expression for the semiclassical Green's function. Inserting this into the expression for the Wigner transform of the Green's function gives

$$G^{+}_{\mathrm{W}}(\boldsymbol{p},\boldsymbol{r};E)=\frac{1}{i\hbar}\left(\frac{1}{2\pi i\hbar}\right)^{(d-1)/2}\times\sum_{\substack{\text{classical}\\ \text{paths}}}\int d\boldsymbol{r}_1\left|D(\boldsymbol{r}-\boldsymbol{r}_1/2,\boldsymbol{r}+\boldsymbol{r}_1/2;E)\right|^{1/2}\times\exp\left[\frac{i}{\hbar}S(\boldsymbol{r}-\boldsymbol{r}_1/2,\boldsymbol{r}+\boldsymbol{r}_1/2;E)-i\frac{\pi}{2}\mu+\frac{i}{\hbar}\boldsymbol{p}\cdot\boldsymbol{\xi}\right]. \tag{22}$$

Using Eqs. (10) and (12) one obtains for the contribution of a given classical path from $\boldsymbol{r}+\boldsymbol{r}_1/2$ to $\boldsymbol{r}-\boldsymbol{r}_1/2$ [compare Fig. 3(a)]

$$\frac{1}{i\hbar}\left(\frac{1}{2\pi i\hbar}\right)^{(d-1)/2}\int d\boldsymbol{r}_1\int\frac{d\boldsymbol{p}\,d\boldsymbol{r}}{(2\pi\hbar)^d}A(\boldsymbol{p}_t,\boldsymbol{r}_t)\,A(\boldsymbol{p},\boldsymbol{r})\times\left|D(\boldsymbol{r}-\boldsymbol{r}_1/2,\boldsymbol{r}+\boldsymbol{r}_1/2;E)\right|^{1/2}\times\exp\left[\frac{i}{\hbar}S(\boldsymbol{r}-\boldsymbol{r}_1/2,\boldsymbol{r}+\boldsymbol{r}_1/2;E)-i\frac{\pi}{2}\mu+\frac{i}{\hbar}\boldsymbol{p}\boldsymbol{r}_1\right]. \tag{23}$$

The integrals over $\boldsymbol{p}$ und $\boldsymbol{r}_1$ are calculated within the stationary phase approximation. The conditions of stationary phase in Eq. (23) are $\boldsymbol{r}_1=0$ and $-(\boldsymbol{p}''+\boldsymbol{p}')/2+\boldsymbol{p}=\boldsymbol{0}$. Hence only closed classical orbits contribute in this approximation. For a given closed classical path [compare Fig. 3(b)] one obtains a contribution of the form

$$\frac{1}{i\hbar}\left(\frac{1}{2\pi i\hbar}\right)^{(d-1)/2}\int d\boldsymbol{r}A(\boldsymbol{p}_t,\boldsymbol{r}_t)\,A(\boldsymbol{p},\boldsymbol{r})\times\left|D(\boldsymbol{r},\boldsymbol{r};E)\right|^{1/2}\exp\left[\frac{i}{\hbar}S(\boldsymbol{r},\boldsymbol{r};E)-i\frac{\pi}{2}\mu\right]. \tag{24}$$

The final integral over $\boldsymbol{r}$ can again be evaluated in a stationary-phase approximation, which ensures that only periodic orbits contribute [compare Fig. 3(c)] The calculation is identical to the original one of Gutzwiller and we only quote the final result for the oscillatory part of $C(E,\hbar\omega)$,

$$\tilde{C}(E,\hbar\omega)=\frac{1}{\pi\hbar}\sum_{p,r}C_p(E,\hbar\omega)\,w_{pr}\,T_p\times\cos\left(\frac{1}{\hbar}rS_p(E)-\frac{\pi}{2}r\mu_p\right), \tag{25}$$

where the sum is over periodic orbits p and their repetitions r, T_p are the periods of the periodic orbits and $S_p(E)$ the respective actions. The semiclassical weights w_{pr} are given by $w_{pr}=1/\sqrt{|\det(M_p^r-1)|}$, where M_p^r are the monodromy matrices. Finally, $C_p(E,\hbar\omega)$ are Fourier transforms of correlation functions along periodic orbits

$$C_p(E,\hbar\omega)=\frac{1}{2\pi\hbar}\int_{-\infty}^{\infty}dt\,\exp(i\omega t)\,C_p(E,t)=\frac{1}{2\pi\hbar}\int_{-\infty}^{\infty}dt\,\exp(i\omega t)\,\frac{1}{T_p}\times\int_0^{T_p}dt'\,A(\boldsymbol{p}_{t+t'},\boldsymbol{r}_{t+t'})\,A(\boldsymbol{p}_{t'},\boldsymbol{r}_{t'}). \tag{26}$$

Since the autocorrelation functions are periodic functions of time with period T_p, they can be expressed as a Fourier sum $C_p(E,t)=\Sigma_\nu\alpha_{p\nu}(E)\exp(i\omega_{p\nu}t)$ with $\omega_{p\nu}=2\pi\nu T_p^{-1}$. This yields

$$C_p(E,\hbar\omega)=\sum_\nu\alpha_{p\nu}(E)\,\delta(\hbar\omega-\hbar\omega_{p\nu}). \tag{27}$$

Finally, we quote the oscillatory contribution to Eq. (5) (see [5] and [17]),

$$d_A(E)=\langle d_A(E)\rangle+\tilde{d}_A(E),$$

$$\tilde{d}_A(E)=\mathrm{Re}\frac{1}{\pi\hbar}\sum_{pr}A_p\,w_{pr}\,T_p$$

$$\times \exp\left(\frac{i}{\hbar} r S_p(E) - i r \frac{\pi}{2} \mu_p\right), \tag{28}$$

where $A_p = T_p^{-1} \int_0^{T_p} dt\, A(\boldsymbol{p}_t, \boldsymbol{r}_t)$ is the average of the observable along the periodic orbit p. This completes the discussion of chaotic systems. In the next section we turn to classically integrable systems.

B. Classically integrable systems

In this section we derive semiclassical approximations for the local densities defined in Eqs. (5) and (6) for classically integrable systems.

1. Semiclassical theory for diagonal matrix elements

We consider the quantum-mechanical density of states

$$d_A(E) = \sum_{mn} \langle \psi_{mn} | \hat{A} | \psi_{mn} \rangle \delta(E - E_{mn}) \tag{29}$$

for integrable systems. Here E_{mn} and $|\psi_{mn}\rangle$ are the eigenvalues and eigenfunctions of the circular quantum billiard. They are labeled in terms of their radial and azimuthal quantum numbers m and n. In terms of the actions $\boldsymbol{I}$, the quantization conditions are [36]

$$I_1 = \oint d\phi\, p_\phi = 2\pi n \hbar\,, \quad I_2 = \oint dr\, p_r = 2\pi (m + 3/4)\hbar\,. \tag{30}$$

With Eq. (30) the density (29) may be written as

$$d_A(E) = \sum_{\boldsymbol{I}} \langle \psi_{\boldsymbol{I}} | \hat{A} | \psi_{\boldsymbol{I}} \rangle \delta[E - H(\boldsymbol{I})], \tag{31}$$

where $|\psi_{\boldsymbol{I}}\rangle$ are the wave functions associated with the quantizing tori $\boldsymbol{I}$. Within the Wigner-Weyl formalism, the matrix elements $\langle \psi_{\boldsymbol{I}} | \hat{A} | \psi_{\boldsymbol{I}} \rangle$ may be expressed as phase-space integrals of the classical observable $A(\boldsymbol{p},\boldsymbol{q})$ times the Wigner function of the corresponding eigenstate $\psi_{\boldsymbol{I}}\rangle$. In action-angle variables, the latter is given by [38] $\delta(\boldsymbol{I} - \boldsymbol{I}')$, and hence

$$\langle \psi_{\boldsymbol{I}} | \hat{A} | \psi_{\boldsymbol{I}} \rangle = \int \frac{d\boldsymbol{\theta}}{(2\pi)^2} A(\boldsymbol{I}, \boldsymbol{\theta}) \equiv A(\boldsymbol{I}). \tag{32}$$

Following Ref. [39], the sum over $\boldsymbol{I}$ is rewritten as an integration, using the Poisson summation formula

$$d_A(E) = \frac{2}{\hbar^2} \sum_{\boldsymbol{M}} \exp\left(i \frac{\pi}{2} \boldsymbol{M}\boldsymbol{\alpha}\right) \times \int d\boldsymbol{I} A(\boldsymbol{I})\, \delta[E - H(\boldsymbol{I})] \exp(2\pi i \boldsymbol{M}\boldsymbol{I}/\hbar). \tag{33}$$

Here, the actions are integrated over $I_1, I_2 > 0$ and $\boldsymbol{M} = (M_1, M_2)$ are vectors on the lattice reciprocal to the EBK lattice (m,n). For a discussion of the phases $\boldsymbol{\alpha}$ see [39]. The first term in Eq. (33), $\boldsymbol{M} = 0$, is just the phase-space average of $A(\boldsymbol{I}, \boldsymbol{\theta})$

$$\langle d_B(E) \rangle = \int \frac{d\boldsymbol{I} d\boldsymbol{\theta}}{(2\pi\hbar)^2} A(\boldsymbol{I}, \boldsymbol{\theta})\, \delta[E - H(\boldsymbol{I})], \tag{34}$$

in analogy with Weyl's rule for the density of state [see Eq. (21)]. For $\boldsymbol{M} \neq 0$, the integral over $\boldsymbol{I}$ is performed in a stationary phase approximation [39,40] and one obtains

$$\tilde{d}_A(E) = \hbar^{-3/2} \mathrm{Re} \sum_{\boldsymbol{M}>0} A_{\boldsymbol{M}} w_{\boldsymbol{M}} \times \exp\left(\frac{i}{\hbar} S_{\boldsymbol{M}}(E) + i \frac{\pi}{2} \mu_{\boldsymbol{M}}\right), \tag{35}$$

where

$$A_{\boldsymbol{M}} = \int \frac{d\boldsymbol{\theta}}{(2\pi)^2} A(\boldsymbol{I}_{\boldsymbol{M}}, \boldsymbol{\theta}). \tag{36}$$

The summation in Eq. (35) is over all rational tori with actions $\boldsymbol{I}_{\boldsymbol{M}}$. The vector $\boldsymbol{M} = (M_1, M_2)$ characterizes their topology, $S_{\boldsymbol{M}}(E)$ and $L_{\boldsymbol{M}}$ are the Maupertuis actions and the lengths of the orbits on the tori $\boldsymbol{M}$. In the case of the circular billiard, one has $L_{\boldsymbol{M}} = 2M_2 \sin(\pi M_1/M_2)$, $S_{\boldsymbol{M}}(E) = \sqrt{2mE} L_{\boldsymbol{M}}$, $w_{\boldsymbol{M}} = (8\pi)^{-1/2} g_{\boldsymbol{M}} L_{\boldsymbol{M}}^{3/2} M_2^{-2} E^{-1/4}$, and the phases $\mu_{\boldsymbol{M}}$ are given by $\mu_{\boldsymbol{M}} = 1/2 - 3M_2$. The factor $g_{\boldsymbol{M}}$ accounts for the twofold degeneracy of tori with finite angular momentum $\pm p_\phi$ which give identical contributions to Eq. (21). Motion along self-retracing orbits on tori with vanishing angular momentum (where $\boldsymbol{M} = r(1,2)$ with $r = 1,2,\ldots$) has $g_{\boldsymbol{M}} = 1$, accordingly.

Equations (35) and (36) provide a semiclassical estimate for the density (5) for integrable systems. In the next section we briefly discuss the case of nondiagonal matrix elements (6).

2. Semiclassical theory for nondiagonal matrix elements

In the present section we give a semiclassical estimate for the density (6) for classically integrable systems. The desired result follows immediately from Eqs. (35) and (36) by replacing $A(\boldsymbol{p},\boldsymbol{r})$ by $A(\boldsymbol{p}_t,\boldsymbol{r}_t)A(\boldsymbol{p},\boldsymbol{r})$, in the same way as Eq. (6) is obtained from Eq. (5) by replacing $\langle \psi_\alpha | \hat{A} | \psi_\alpha \rangle$ by $\langle \psi_\alpha | \hat{A}_t \hat{A} | \psi_\alpha \rangle = \Sigma_\beta |\langle \psi_\alpha | \hat{A} | \psi_\beta \rangle|^2 \exp[i(E_\alpha - E_\beta)t/\hbar]$. One obtains

$$C(E, \hbar\omega) = \langle C(E, \hbar\omega) \rangle + \tilde{C}(E, \hbar\omega) \tag{37}$$

with

$$\langle C(E, \hbar\omega) \rangle \simeq \frac{1}{2\pi\hbar} \int dt \exp\left(\frac{i}{\hbar}\omega t\right) \times \int \frac{d\boldsymbol{I} d\boldsymbol{\theta}}{(2\pi\hbar)^2} A(\boldsymbol{I}, \boldsymbol{\theta} + \boldsymbol{\omega} t)\, A(\boldsymbol{I}, \boldsymbol{\theta})\, \delta[E - H(\boldsymbol{I})] \tag{38}$$

$$\tilde{C}(E,\hbar\omega)=\hbar^{-3/2}\sum_{M>0} C_M(E,\hbar\omega)\, w_M \times\cos\left(S_M(E)+i\frac{\pi}{2}\mu_M\right), \tag{39}$$

where

$$C_M(E,\hbar\omega)=\int\frac{dt}{2\pi\hbar}\exp\left(\frac{i}{\hbar}\omega t\right)\times\int\frac{d\boldsymbol{\theta}}{(2\pi)^2}A(\boldsymbol{I}_M,\boldsymbol{\theta}+\boldsymbol{\omega}_M t)\,A(\boldsymbol{I}_M,\boldsymbol{\theta})\,. \tag{40}$$

The phase-space observables are periodic functions of the angle variables $\boldsymbol{\theta}$ and can be expanded as follows:

$$A(\boldsymbol{I}_M,\boldsymbol{\theta})=\sum_{\boldsymbol{\nu}} A_{\boldsymbol{\nu}}(\boldsymbol{I})\exp(i\boldsymbol{\nu}\cdot\boldsymbol{\theta})\,. \tag{41}$$

This gives, using $\omega_{\boldsymbol{\nu}}(\boldsymbol{I})=\boldsymbol{\nu}\cdot\boldsymbol{\omega}(\boldsymbol{I})$,

$$\langle C(E,\hbar\omega)\rangle\simeq\sum_{\boldsymbol{\nu}}\int d\boldsymbol{I}\,|A_{\boldsymbol{\nu}}(\boldsymbol{I})|^2\,\delta[\hbar\omega-\hbar\omega_{\boldsymbol{\nu}}(\boldsymbol{I})]\times\delta[E-H(\boldsymbol{I})] \tag{42}$$

and

$$C_M(E,\hbar\omega)=\sum_{\boldsymbol{\nu}}|A_{\boldsymbol{\nu}}(\boldsymbol{I}_M)|^2\,\delta[\hbar\omega-\hbar\omega_{\boldsymbol{\nu}}(\boldsymbol{I}_M)]\,. \tag{43}$$

This completes the semiclassical analysis of Eqs. (5) and (6), for integrable as well as for chaotic, ergodic systems. In the following sections we compare the semiclassical theory with results of quantum-mechanical calculations.

IV. RESULTS FOR DIAGONAL MATRIX ELEMENTS

In the present section we discuss the sum rules (28) and Eqs. (34),(35) for diagonal matrix elements and compare numerical results for the system introduced in Sec. II with the theory of Sec. III. We will first discuss the smooth contributions (which are insensitive to the nature of the classical dynamics) and then the oscillatory contributions separately for chaotic and integrable systems. We choose units in which $m=1/2$ and $\hbar=1$.

A. The Weyl part

According to Eqs. (28) and (34) Weyl's rule approximates the mean density of matrix elements, just as the smooth part of the density of states $d(E)=\Sigma_\alpha\delta(E-E_\alpha)$ is asymptotically given by [2]

$$\langle d(E)\rangle=\frac{A}{4\pi}-\frac{L}{8\pi}\frac{1}{\sqrt{E}}. \tag{44}$$

Here A is the area of the billiard and L is its circumference. The first term corresponds to Weyl's rule. The second term is a perimeter correction. In the presence of diagonal matrix elements, the perimeter term is given by the average of $A(\boldsymbol{r})$ along the boundary, $\langle A\rangle_{\rm bdy}$,

$$\langle d_A(E)\rangle=\langle A\rangle_{\rm mc}\frac{A}{4\pi}-\langle A\rangle_{\rm bdy}\frac{L}{8\pi}\frac{1}{\sqrt{E}}. \tag{45}$$

For observables of the form $A(\boldsymbol{r})$ this can be shown using the method of images [41]. In the presence of symmetries, Eq. (44) is further modified and holds separately for each symmetry class [2]. The symmetry reduced version of Eq. (45) is obtained analogously and the perimeter terms are denoted by $\langle A\rangle^{\pm}_{\rm bdy}$ for positive and negative y parity. We have verified Eq. (45) by calculating the first 1250 eigenvalues of positive parity and the corresponding diagonal matrix elements $\langle\psi_\alpha|\hat{A}|\psi_\alpha\rangle$ as a function of the deformation parameter a. We have taken $A=x$. In scaled variables, Eqs. (44) and (45) are replaced by

$$\langle d(z)\rangle=\frac{A}{2\pi}z-\frac{L}{4\pi}, \tag{46}$$

$$\langle d_A(z)\rangle=\langle A\rangle_{\rm mc}\frac{A}{2\pi}z-\langle A\rangle_{\rm bdy}\frac{L}{4\pi} \tag{47}$$

(see Appendix A). For the dipole operator, $A=x$, the microcanonical average is easily verified to be $\langle x\rangle_{\rm mc}=a(2+a^2/2)/(2+a^2)$. The elliptic integrals arising in the average of $A(\boldsymbol{r})$ along the boundary have to be evaluated numerically. Figure 4 shows the numerical coefficients of a polynomial fit to the mean densities $\langle d(z)\rangle$ and $\langle d_A(z)\rangle$ as a function of a. Also shown are the analytical values given above. The close agreement shows that the mean part of $\langle d_A(z)\rangle$ can be determined accurately, which is important for the analysis of the fluctuating part. We note that both $\langle x\rangle_{\rm mc}$ as well as $\langle x\rangle_L$ tend to zero for $a\to 0$ for symmetry reasons.

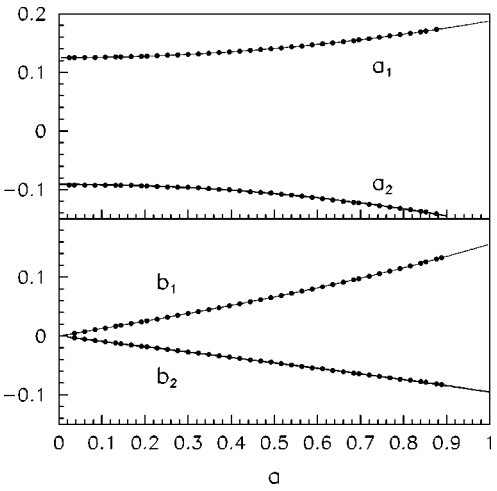

FIG. 4. Coefficients of a polynomial fit of $\langle d(z)\rangle$ and $\langle d_A(z)\rangle$ as a function of the deformation parameter a. (a) shows the density of states $\langle d(z)\rangle\sim a_1 z+a_0$. (b) shows $\langle d_A(z)\rangle\sim b_1 z+b_0$. Shown are the analytical estimates (solid lines) as well as results of numerical calculations (●), as described in the text.

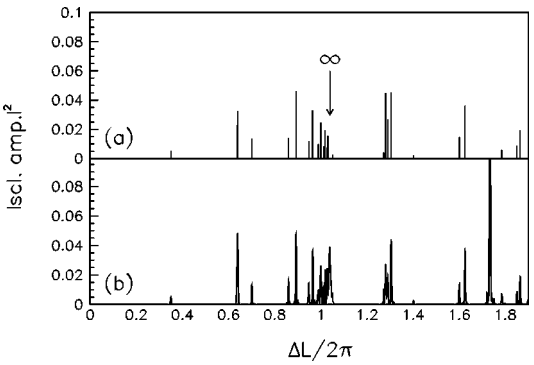

FIG. 5. Modulus squared of the Fourier transform of $\tilde{d}_A(z)$ (with $A=x$) in comparison with its semiclassical approximation (49) for $a=1/2$ and π^+. (a) shows the semiclassical approximation. The perimeter of the billiard — where the lengths of the whispering gallery orbits accumulate — is marked by ∞. (b) shows the quantum spectrum.

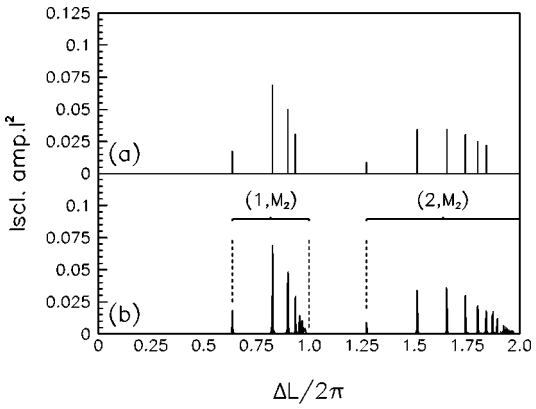

FIG. 6. Fourier transformation of $z^{-1/2}\tilde{d}_A(z)$ for $A=\boldsymbol{r}^2$ in the integrable case. (a) shows the semiclassical theory as calculated from Eq. (50). The peaks are labeled by the vector $\boldsymbol{M}$ characterizing the topologies of the corresponding tori. (b) shows the corresponding quantum-mechanical amplitudes.

B. Periodic-orbit contributions

It has been shown in Sec. III how oscillatory contributions to Eq. (5) arise semiclassically as sums over periodic orbits. In this section we discuss these contributions for the classically chaotic and integrable cases. In what follows we always work with scaled variables, as defined in Appendix A.

1. Chaotic case

For a scaling system, Eq. (28) is conveniently rewritten as follows. We define

$$d_A(z)=\sum_\alpha \langle\psi_\alpha|\hat{A}|\psi_\alpha\rangle\,\delta(z-z_\alpha)\,, \tag{48}$$

where $z_\alpha=\sqrt{E_\alpha}$. According to Appendix A,

$$\tilde{d}_A(z)=\frac{1}{\pi}\mathrm{Re}\sum_{p,r} w_{pr}A_pL_p\exp[r(izL_p-i\pi\mu_p/2)], \tag{49}$$

where $A_p=L_p^{-1}\int_0^{L_p}dsA(\boldsymbol{p}_s,\boldsymbol{r}_s)$ is the average of the observable $A(\boldsymbol{p},\boldsymbol{r})$ around the periodic orbit p. In order to analyze the periodic-orbit contributions to $d_A(z)$, we subtract the Weyl part and Fourier transform the fluctuating part with respect to z. In scaled variables, the periodic orbit contributions (49) appear as a Fourier series in z, the periodic orbits stand out as peaks located at their respective lengths L_p, their amplitudes are given by $A_p\,w_{pr}$. In the following we take $A=x$, such that the amplitudes A_p are z independent. Figure 5 shows the Fourier transform of the oscillating part of $d_A(z)$ for $\hat{A}=x$. It is well described by the semiclassical approximation (vertical bars), provided the difference in length of the orbits is large compared to the quantal resolution. There are cases where this condition is not met. One example is the unstable horizontal orbit 2 with length $L/2\pi=0.6366$. It cannot be resolved from the stable orbit 4^2 bifurcated from 2 at $a=\sqrt{2}-1$. The latter has the length $L/2\pi=0.6406$ at $a=1/2$. The same is the case for the pair of six-hit orbits 6^2 and 6^{2a}, whose length are almost degenerate at $a=1/2$. Another example is the infinite family of whispering gallery orbits originating from resonant tori with winding number $1/n$. Although the shortest orbits ($n=3,4,5$) may still be resolved, their actions converge to the circumference of the billiard as $1/n^2$ ($n\to\infty$) and are no longer resolvable. In Fig. 5, the circumference is indicated by the symbol ∞. Note that the quantum Fourier amplitudes decay to zero as the circumference is approached (at $L/2\pi=1.063\,544$ at $a=1/2$). The reason is that at finite z, the wave functions cannot be localized arbitrarily close to the boundary due to Dirichlet boundary conditions. Instead, they are localized near some orbit with finite n, with n increasing with z. Thus, due to the finiteness of the numerical spectrum, whispering gallery orbits with finite n contribute.

2. Integrable systems

In the present section we discuss periodic orbit contributions to the density (5) for integrable systems. In scaled variables,

$$\tilde{d}_A(z)=\sqrt{\frac{1}{2\pi}}\sum_{\boldsymbol{M}>0} A_{\boldsymbol{M}}g_{\boldsymbol{M}}L_{\boldsymbol{M}}^{3/2}M_2^{-2}\sqrt{z}\times\cos\left(zL_{\boldsymbol{M}}+\frac{\pi}{4}-\frac{3\pi}{2}M_2\right). \tag{50}$$

In order to check the prediction (50), we have calculated $\tilde{d}_A(z)$ quantum mechanically for the observable $A=\boldsymbol{r}^2$. For this observable, $A_{\boldsymbol{M}}=[1+2\cos^2(\pi M_1/M_2)]/3$ is z independent. In order to eliminate the z dependence in the amplitudes in Eq. (50), it is convenient to consider $z^{-1/2}\tilde{d}_A(z)$. As before, the Weyl part has to be subtracted. We have fitted $z^{-1/2}\langle d_A(z)\rangle$ and subtracted the mean part numerically. The Fourier spectrum of $z^{-1/2}\tilde{d}_A(z)$ is shown in Fig. 6. We observe good agreement between the quantum-mechanical and the semiclassical spectrum for lengths sufficiently far away from integer multiples of the circumference. A uniform approximation designed to improve the semiclassical length spectrum in the vicinity of the circumference was discussed in [42].

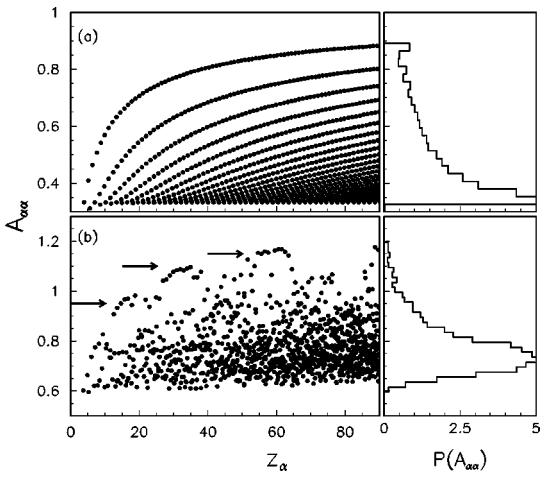

FIG. 7. Diagonal matrix elements of $\boldsymbol{r}^2$. Top: Matrix elements as a function of the corresponding scaled energies z_α for the integrable case ($a=0$). Bottom: the same, but for the chaotic case ($a=1/2$). Also shown are the corresponding distributions.

C. Distributions

In the preceding two subsections we have discussed the semiclassical evaluation of a sum rule for diagonal matrix elements. Expectation values in chaotic quantum systems are constrained by this sum rule and on energy scales larger than the mean level spacing this leads to deviations from random matrix statistics [5]. Semiclassically, these deviations are due to short periodic orbits.

In addition, there are other ways in which expectation values may be affected by classical short-time dynamics. Even in classically chaotic systems, for instance, substantial deviations from Gaussian fluctuations can occur as pointed out in the introduction. Fig. 7(a) shows diagonal matrix elements of $A=\boldsymbol{r}^2$ for the circular quantum billiard as a function of their energies z_{mn}. We observe that the matrix elements fall on lines of constant radial quantum number m, as expected for the observable $\boldsymbol{r}^2$ in an integrable system. This behavior is quite different from the chaotic case [see Fig. 7(b)], where the matrix elements scatter irregularly around the microcanonical phase space average $\langle A\rangle_{\rm mc}$ (in agreement with Shnirelman's theorem). This difference between the integrable and the chaotic case reflects the different nature of the wave functions in the two cases. While the chaotic wave functions are expected to be more or less equally weighted in configuration space, $\int_D d\boldsymbol{r}|\psi_\alpha(\boldsymbol{r})|^2\sim{\rm vol}(D)$, the regular wave functions associated with a particular torus are strongly localized radially between the radius of the corresponding caustic

We emphasize that also in the ergodic case [Fig. 7 (bottom)] we observe strings of diagonal matrix elements (with $A_{\alpha\alpha}\gtrsim 1$). These are marked by arrows and are associated with matrix elements between eigenstates localized in the vicinity of whispering gallery orbits. The observable $\boldsymbol{r}^2$ was chosen because it couples strongly to whispering gallery motion.

Also shown in Fig. 7 are histograms of the diagonal matrix elements of $A=\boldsymbol{r}^2$ for the integrable ($a=0$) and the chaotic case ($a=1/2$). In both cases, the shapes of the distributions are strongly non-Gaussian and reflect the organization of classical phase space. For $a=0$, the distribution is determined by the distribution of tori on the energy shell. For $a=1/2$, the non-Gaussian shoulder is caused by states localized in the vicinity of the whispering gallery motion, to which the observable $\boldsymbol{r}^2$ is particularly sensitive.

V. RESULTS FOR NONDIAGONAL MATRIX ELEMENTS

A. Classically chaotic case

1. Scaling behavior

As before we make use of the fact that the billiard system introduced in Sec. II is a scaling system, in the sense discussed in Appendix A. We introduce a scaled version of the density (6),

$$C(z,\Delta z)=\sum_{\alpha\beta}|\langle\psi_\alpha|\hat{A}|\psi_\beta\rangle|^2\,\delta_\eta(z-z_\alpha)\,\delta_\epsilon(\Delta z-z_\alpha+z_\beta) \tag{51}$$

(Appendix A), where $\Delta z=\hbar\omega/2z$ is a scaled frequency, $z_\alpha=\sqrt{E_\alpha}$ and $\delta_\eta(z)=\eta/[\pi(x^2+\eta^2)]$. The density (51) has a particularly transparent semiclassical expansion,

$$C(z,\Delta z)=\langle C(z,\Delta z)\rangle + \frac{1}{\pi}{\rm Re}\sum_{p,r} C_p(\Delta z)\,L_p\,w_{pr} \times\exp[r(izL_p-i\pi\mu_p/2-\eta L_p)]\,. \tag{52}$$

The $C_p(\Delta z)$ are analogous to the quantities $C_p(E,\hbar\omega)$ defined in Eq. (26),

$$C_p(\Delta z)=\frac{1}{2\pi}\int_{-\infty}^{\infty}dL\,C_p(L)\exp(i\Delta zL-\epsilon|L|), \tag{53}$$

and $C_p(L)$ is a scaled autocorrelation function (Appendix A) around the periodic orbit p. Since we are working with scaled variables, the functions $C_p(\Delta z)$ are independent of z. Since the same applies to the monodromy matrix, the semiclassical amplitudes in Eq. (52) are energy independent. The smooth contribution also simplifies considerably in scaled variables. It can be written as

$$\langle C(z,\Delta z)\rangle=\langle d(z)\rangle\frac{1}{2\pi}\int_{-\infty}^{\infty}dL\,C^{\rm cl}(L)\exp(i\Delta zL-\epsilon|L|)\,. \tag{54}$$

where $C^{\rm cl}(L)$ is a ergodic correlation function in scaled variables. This implies that the z and the Δz dependence of $C(z,\Delta z)$ factorizes in scaled variables,

$$\langle C(z,\Delta z)\rangle\sim z^{4\gamma}\langle d(z)\rangle\,f(\Delta z)\,, \tag{55}$$

where $f(\Delta z)$ is a z-independent scaling function and γ is the exponent describing the scaling of the observable $\hat{A}$, namely, $A(\boldsymbol{p},\boldsymbol{r})=E^\gamma A_0(\boldsymbol{p}_0,\boldsymbol{r}_0)$ as discussed in Appendix A. Figure 8 shows $C(z,\Delta z)$ for $\hat{A}=\hat{x}$ for different values of z. For $\hat{A}=\hat{x}$, one has $\gamma=0$ and hence the curves in Fig. 8 fall onto one single curve if rescaled with $\langle d(z)\rangle^{-1}$ (inset). The

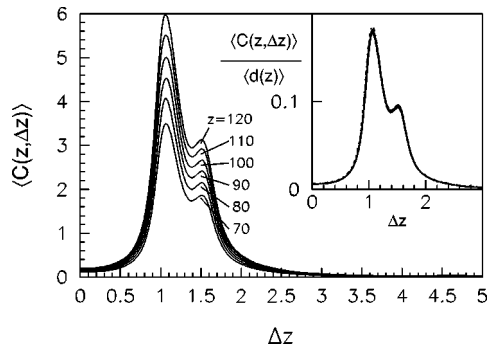

FIG. 8. Scaling of $C(z,\Delta z)$ for $A=x$ with $\langle d(z)\rangle$. Shown is the original spectral function with z centered around $z=70,80,90,100,110,120$ (above) and a rescaled according to $C(z,\Delta z)\,\langle d(z)\rangle^{-1}$ (below).

z-independent curves agree well with their semiclassical approximations given by the Fourier transform of the ergodic autocorrelation function $C^{\rm cl}(L)$ as predicted by Eq. (54).

The factorization of Eq. (54) into a z-dependent part given by $\langle d(z)\rangle$ and a Δz-dependent part allows us to integrate over z, weighted with $\langle d(z)\rangle^{-1}$ in order to obtain an energy-independent expression, i.e.,

$$(z_{\max}-z_{\min})^{-1}\int_{z_{\min}}^{z_{\max}} dz\, C(z,\Delta z)\langle d(z)\rangle^{-1}.$$

This is shown in Fig. 9 for $\hat{A}=\hat{p}_x/z$. In this case, $\gamma=1/2$ and dividing p_x by z serves to remove the factor of $z^{4\gamma}$ in Eq. (55).

Apart from modulations at small values of Δz, $C(z,\Delta z)$ decays as Δz increases. This decay is slow, $C(z,\Delta z)\sim\Delta z^{-\nu}$ and $\nu>0$. For $\hat{A}=\hat{p}_x/z$, we have $C(z,\Delta z)\sim\Delta z^{-2}$, and for $\hat{A}=x$ we have $\nu=4$. This decay is of course typical for billiards, where the dynamics is discontinuous at the boundary. The classical correlation function of a smooth observable $A(\boldsymbol{p}_s,\boldsymbol{r}_s)$ for motion in a billiard has discontinuous derivatives due to the change of direction when the particle collides with the boundary. If $A(\boldsymbol{p}_s,\boldsymbol{r}_s)$ has discontinuities in its nth derivative, the Fourier transform of its correlation function decays as $\Delta z^{-2(n+1)}$ for large Δz. We note that for $A=x$ we have $n=1$ and for $A=p_x/z$ we have $n=0$, which explains the observed decay.

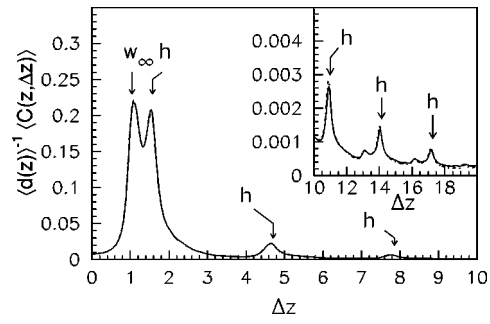

FIG. 9. Comparison between the z-integrated function $(z_{\max}-z_{\min})^{-1}\int dz\, d(z)^{-1}\,C(z,\Delta z)$ for $A=p_x/z$ and the semiclassical approximation (54). The resonances are marked according to their nature, h marks the resonances due to motion in the vicinity of the horizontal orbit 2, w_∞ marks the resonance due to motion in the vicinity of the whispering gallery orbits. The inset shows the same, but for larger values of Δz.

2. Classical localization

In the present section we discuss the origin and interpretation of the fluctuations observed in Figs. 8 and 9. The quantum densities in Figs. 8 and 9 exhibit strong modulations as a function of Δz, superposed onto a smooth decay. Classically, these modulations may be understood as a consequence of nonuniformity of phase space. Generically, the rate of divergence varies locally over phase space with minima near the shortest periodic orbits. The ergodic trajectory, which explores the whole energy shell for infinite time, may be trapped in the neighborhood of stable or weakly unstable orbits for some finite time. The correlation function $C_p(L)$ along a periodic orbit is periodic with L_p. Due to short-time periodic motion the ergodic correlation function also shows quasiperiodic behavior, at least for small L. As a result the Fourier transform has peaks at integer multiples of $\Delta z=2\pi/L_p$.

Let us describe this in more detail for the case $A=p_x/z$ (see Fig. 9), where the correlation functions along periodic orbits may be evaluated analytically. The second peak in Fig. 9 is caused by quasiperiodic motion in the vicinity of the unstable horizontal orbit 2 (with $L_p/2\pi=0.6366$) and the stable orbit 4^2 (with $L_p/2\pi=0.6406$) bifurcated from it. Denoting the angle between the trajectory and the x-axis by ψ ($\psi=0$ for the horizontal orbit), the autocorrelation functions of $A=p_x/z$ along 2 and 4^2 read $C_p(L)=[1-4L/L_p]\cos^2\psi$ for $0\leqslant L\leqslant L_p/2$ and $C_p(L+L_p/2)=-C_p(L)$. Their Fourier transforms shows maxima at odd repetitions of $2\pi/L_p$. Since the lengths of both orbits are almost degenerate at $a=1/2$ (the orbit 4^2 also contributes with half its length if in a single parity subspace), their contributions to the Fourier transform of $C^{\rm cl}$ are indistinguishable. The main peak is located near $\Delta z=1.55$ as can be seen from the figure. The first large peak may be attributed to the infinite family of whispering gallery orbits n, which appear when rational tori with winding number $1/n$ are destroyed. At $a=1/2$, their lengths converge to the circumference of the billiard as $\sim(1-c/n^2)$ with $c>0$. Their Lyapunov exponent increases logarithmically with n, the number of hits on the boundary. This is shown in Fig. 10 where the Lyapunov exponents of the whispering gallery orbits are plotted as a function of the number n of hits on the boundary. The main contribution to the ergodic correlation function thus comes from the shorter, less unstable orbits of the family. Indeed, the maximum in $C(z,\Delta z)$ is found near $\Delta z=1.06$ corresponding to a mean length $L/2\pi=0.94$ or $n\approx 4$.

A more compelling proof of the origin of the resonance structure in the Fourier transform of classical correlation functions has been given in [43]. The main idea is to decompose the phase space into cells of equal size and to calculate the contribution of each cell to the spectrum of the ergodic correlation function at the given (peak) frequency separately. Following [43], we may write

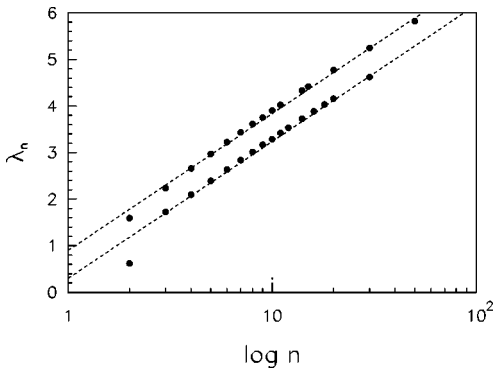

FIG. 10. Lyapunov exponents λ_n for the whispering gallery orbits for $a=1/2$ as a function of the number n of hits at the boundary. There are two kinds of whispering gallery orbits, inverse hyperbolic ones (n in table I) and hyperbolic ones (n^1 in Table I). The dashed lines are fits to $\lambda_n = a + b \ln n$.

$$\int_{-L_c}^{L_c} dL C^{\mathrm{cl}}(L)\exp(i\Delta z L) \approx \frac{1}{N_{\mathrm{cell}}}\sum_{\mathrm{cells}} \langle A(0)\rangle_{\mathrm{cell}} \times \int_{-L_c}^{L_c} dL \langle A(L)\rangle_{\mathrm{cell}} \exp(i\Delta z L), \qquad (56)$$

where $\langle\ \rangle_{\mathrm{cell}}$ denotes an average over initial conditions within a phase-space cell. If we followed the individual trajectories for long enough ($L_c \to \infty$), every phase-space cell would contribute equally to the Fourier transform at any frequency. In order to obtain information about subregions in phase space one has to choose L_c sufficiently small and study the short-time correlations of the cells. In practice, we choose L_c about ten times the length of the shortest periodic orbits, i.e., $L_c = 20$. We restrict ourselves to the surface of section and plot the modulus of the cell amplitudes at fixed scaled frequency Δz. The surface of section is parametrized as follows. We choose the polar angle ϕ to parametrize the x axis. The y coordinate is given by $\sin\chi$ where χ is the angle of incidence at the boundary [44]. The result is shown in Fig. 11 for $\Delta z = 1.5$ (left) and $\Delta z = 1.0$ (right). At $\Delta z = 1.5$ we find highest intensity around the fixed points of the stable orbit 4^2. Regions of high intensity extend to the fixed points of the unstable horizontal orbit 2. They are delineated by the manifolds of the shortest unstable periodic orbits (compare Fig. 11).

At $\Delta z = 1.0$, the picture changes completely. We now find high density around the fixed points of the whispering gallery orbits, with highest intensity around $n=4$ and 5 in accordance with the location of the maximum in Figs. 8 and 9 near $\Delta z = 1.06$ (see above). Qualitatively, we observe that the high-intensity regions tend to follow the line of fixed points and their invariant manifolds (compare Fig. 11).

The above discussion shows that short-time quasiperiodic motion which leads to localization of the classical flow in subregions of phase space, is responsible for the resonance structure in the Fourier transform of the classical ergodic autocorrelation function.

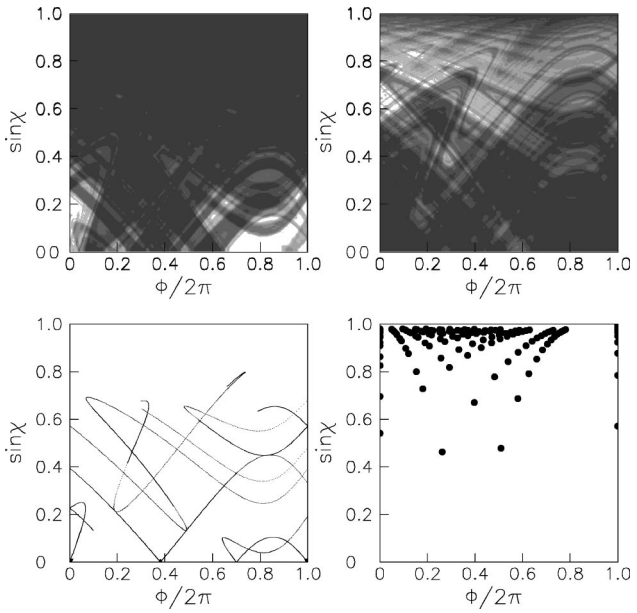

FIG. 11. Classical contribution of phase space cells to the Fourier transform of the ergodic correlation function $C^{\mathrm{cl}}(L)$ at $\Delta z = 1.5$ (left) and $\Delta z = 1.0$ (right) according to Eq. (56). Also shown are invariant manifolds of the shortest periodic orbits (left) and fixed points of the whispering gallery orbits (right).

3. Quantum localization

In the preceding section we have analyzed the resonances in the classical autocorrelation function. Equation (54) allows us to discuss the analogous phenomenon in quantum mechanics.

A corresponding phenomenon of quantum localization has indeed been identified in the form of scars, i.e., higher than average probability distribution of wave functions along isolated unstable periodic orbits. A wave packet started along an unstable periodic orbit would travel around it for some finite time before spreading all over phase space, the sooner the more unstable the underlying orbit. It is possible to quantize the motion parallel to the orbit [45] approximately. It shows in particular that subsequent scars of the same orbit with length L_p are separated by $\Delta z \approx 2\pi/L_p$. If their overlap matrix elements is higher than average, the corresponding $C(z,\Delta z)$ should have a pronounced peak at this value of Δz. We have found strongly scarred wave functions at $a=1/2$, which are localized around the triangular orbit 3 and the orbit 4^2 bifurcated from it and in the vicinity of the family of whispering gallery orbits, see Fig. 12. Although the orbit 4^2 is stable, the localized wave function may well be termed scars, since the stable region around the orbit is much too small to quantize individual states, at least for the energies considered here.

We have analyzed nondiagonal matrix elements of the observable $A = \boldsymbol{r}^2$ between scarred states and between irregular states. In keeping with the above analysis we have found that nondiagonal matrix elements between scarred whispering gallery states are considerably larger than those between irregular states or between a scarred and an irregular state. This shows that inhomogeneities in classical phase space lead to interesting features in the quantum-mechanical density (6), as exemplified in Figs. 8, 9, and 11. We emphasize

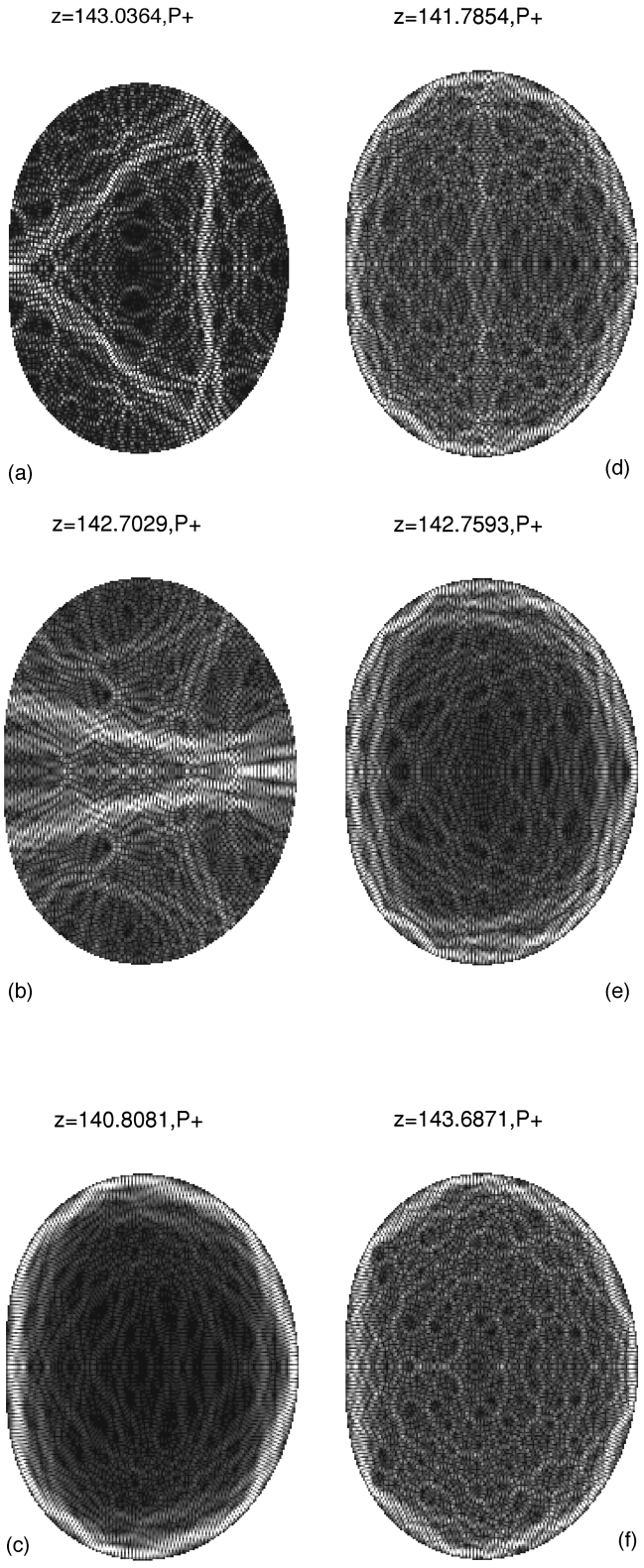

FIG. 12. Some examples of wave functions scarred by short periodic orbits, (a) triangular orbit 3 (compare Fig. 2), (b) stable orbit 4^2, (c), (d), (e) and (f) whispering gallery orbits n. In the cases (c), . . . ,(f), note that subsequent scars are separated by $\simeq 2\pi/L_p$, where L_p denotes the length of the scarring orbit.

that other quantities, such as the distribution of nearest-neighbor level spacings in Fig. 1 show no or little sign of inhomogeneities in classical phase space. The quantity defined in Eq. (6) is therefore particularly suited to analyze the effect of classical phase-space localization in quantum mechanics.

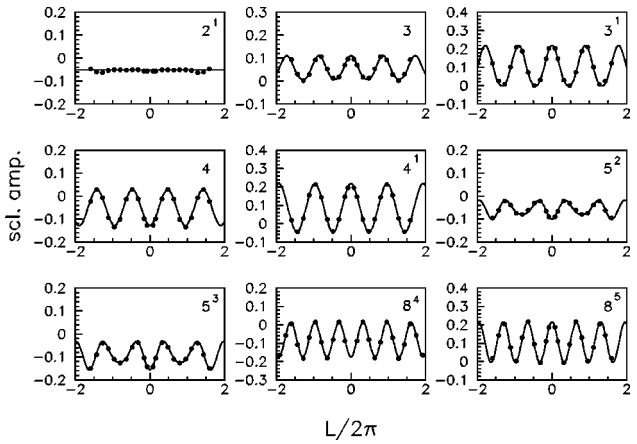

FIG. 13. Real part of the Fourier transform of $\tilde{C}(z,L)$ with respect to z for $A=x$ (●) in comparison with its semiclassical approximation (solid lines).

4. Periodic orbits

According to Eq. (52), the contribution of a particular periodic orbit to $\tilde{C}(z,\Delta z)$ is weighted by the correlation function of $A(\boldsymbol{p},\boldsymbol{r})$ along the orbit. In the following we discuss contributions of individual periodic orbits and compare the semiclassical predictions with exact quantum results. To this end, we Fourier transform the fluctuating part of Eq. (52) with respect to z and Δz. The variable conjugate to Δz is taken to be L, and the variable conjugate to z is ΔL, following the convention introduced in [16]. According to Eq. (52), the function $\tilde{C}(\Delta L,L)$ exhibits peaks as a function of ΔL at the lengths of the periodic orbits L_p. The amplitudes depend parametrically on the length L, which is conjugate to the scaled frequency Δz. The dependence on L is given by the periodic orbit correlation function $C_p(L)$. In order to compare the semiclassical formulas with the results of numerical quantum calculations, we proceed as follows. For fixed L we determine the amplitude of the quantum Fourier transform at $\Delta L=L_p$. For each orbit, the results for different L values are collected together and compared with the semiclassical amplitudes modulated by the periodic orbit correlation functions. The results, for $\hat{A}=\hat{x}$, are shown in Fig. 13. In all cases, the quantum as well as the semiclassical amplitudes are shown. We find excellent agreement between the quantum and the semiclassical amplitudes.

B. Classically integrable systems

In the preceding section, we discussed classical and periodic-orbit contributions to the density (6) for classically chaotic systems. In the present section we analyze integrable systems. In scaled variables one has

$$C(z,\Delta z)=\langle C(z,\Delta z)\rangle + \sqrt{\frac{1}{2\pi}}\mathrm{Re}\sum_{\boldsymbol{M}\neq 0} g_{\boldsymbol{M}} C_{\boldsymbol{M}}(\Delta z) L_{\boldsymbol{M}}^{3/2} M_2^{-2}\sqrt{z} \times \exp\left[izL_{\boldsymbol{M}} + i\frac{\pi}{4} - i\frac{3\pi}{2}M_2 - \eta L_{\boldsymbol{M}}\right]. \quad (57)$$

$C_{\boldsymbol{M}}(\Delta z)$ denotes the Fourier transform of the autocorrelation function of the observable A on the rational torus $\boldsymbol{M}$,

$$C_{\boldsymbol{M}}(\Delta z)=\frac{1}{2\pi}\int_{-\infty}^{\infty} dL\, C_{\boldsymbol{M}}(L)\exp(i\Delta z L-\epsilon|L|), \quad (58)$$

$$C_{\boldsymbol{M}}(L)=\int \frac{d\boldsymbol{\theta}}{(2\pi)^2}A(\boldsymbol{I}_{\boldsymbol{M}},\boldsymbol{\theta})A(\boldsymbol{I}_{\boldsymbol{M}},\boldsymbol{\theta}+\boldsymbol{\omega}L/2z). \quad (59)$$

In the following we discuss classical and periodic-orbit contributions separately.

1. Weyl contributions: asymptotic analysis

In this section we calculate the Weyl contribution to $C(z,\Delta z)$ for integrable systems analytically. This is possible as an asymptotic expansion for large L, where L is the variable conjugate to Δz. We will show that in general, $\langle C(z,L)\rangle \simeq \langle d(z)\rangle L^{-(d-1)/2}$. In scaled variables, as a function of L, the Weyl part is given by

$$\langle C(z,L)\rangle=\frac{1}{(2\pi)^2}\int d\boldsymbol{\theta}\, d\boldsymbol{I}\, B(\boldsymbol{I},\boldsymbol{\theta}) \times B(\boldsymbol{I},\boldsymbol{\theta}+\boldsymbol{\omega}L/2z)\,\delta[z-\sqrt{H(\boldsymbol{I})}]\,. \quad (60)$$

In order to evaluate this integral, we introduce new Cartesian coordinates $\boldsymbol{I}\to\boldsymbol{\xi}=(\xi_1,\xi_2)$ such that ξ_2 is always tangential to the curve $H(\boldsymbol{I})=z^2$. Performing the integral over ξ_1 yields a line integral along the curve $H(\boldsymbol{I})=z^2$. We parametrize this curve by $I_2=g_z(I_1)$. Using $|\partial H/\partial I_2| = \omega_2 = 2\pi z/\sqrt{1-r_{\min}^2}$ and $I_1=r_{\min}z$ we obtain

$$\langle C(z,L)\rangle=\langle d(z)\rangle\frac{4}{\pi}\int_0^1 dr_{\min}\sqrt{1-r_{\min}^2} \times\int\frac{d^2\theta}{(2\pi)^2}B(\boldsymbol{I},\boldsymbol{\theta})B(\boldsymbol{I},\boldsymbol{\theta}+\boldsymbol{\omega}L/2z)\,. \quad (61)$$

The symmetry $p_\phi\to -p_\phi$ is taken into account by an additional factor of 2. Since $\boldsymbol{\omega}\sim 2z$, Eq. (61) explicitly exhibits the scaling property of $\langle C(z,\Delta z)\rangle$ discussed above, namely, that the z and L dependences factorize.

Equation (61) can be evaluated further most easily for operators with rotational symmetry. Consider for instance $A=\boldsymbol{r}^2$. In this case we have

$$\int\frac{d\boldsymbol{\theta}}{(2\pi)^2}B(\boldsymbol{I},\boldsymbol{\theta})B(\boldsymbol{I},\boldsymbol{\theta}+\boldsymbol{\omega}L/2z) = \tfrac{1}{6}[1-L^2(L-2\sqrt{1-r_{\min}^2})^2]+\tfrac{2}{15}(\tfrac{1}{2}+2r_{\min}^2)^2. \quad (62)$$

A numerical evaluation of this integral, using Eq. (62), is shown in Fig. 14(a) together with the corresponding quantum-mechanical data. We observe good agreement between the quantum-mechanical data and the corresponding semiclassical approximation. Figure 14(b) shows the same data, but for the chaotic case. Here, the ergodic autocorrelation function is evaluated numerically as a time average over a very long trajectory. Both autocorrelation functions exhibit characteristic oscillations with frequency $\Delta z\sim\pi$. In comparison with its chaotic counterpart, the integrable autocorrelation function exhibits a highly regular structure. In both cases, the envelope decays to a constant as $L\to\infty$. There are, however, important differences. These will be discussed in the following.

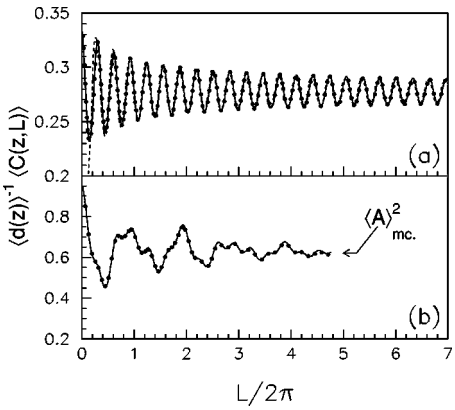

FIG. 14. Classical autocorrelation function (solid line) for $A=\boldsymbol{r}^2$, and the result of a quantum-mechanical calculation (●). Shown are two cases, (a) the integrable case and (b) the chaotic case ($a=1/2$) for comparison.

In the integrable case, the envelope of the autocorrelation function decays according to $\sim 1/\sqrt{L}$. Using Eqs. (41) and (42), we rewrite Eq. (61) as

$$\langle C(z,L)\rangle=\langle d(z)\rangle\frac{4}{\pi}\sum_{\boldsymbol{\nu}}\int_0^1 dr_{\min}\sqrt{1-r_{\min}^2}\,|A_{\boldsymbol{\nu}}|^2 \times\exp(i\boldsymbol{\nu}.\boldsymbol{\omega}L/2z)\,. \quad (63)$$

Here $A_{\boldsymbol{\nu}}$ are the Fourier coefficients of the observable $A(\boldsymbol{I},\boldsymbol{\theta})$. In the present case, they are functions of $r_{\min}$, as are the frequencies $\boldsymbol{\omega}$. For a rotationally invariant observable, such as $A=\boldsymbol{r}^2$, the Fourier series is one dimensional. For $A=\boldsymbol{r}^2$ we have

$$A_\nu(r_{\min})=\begin{cases}\dfrac{1}{3}(1+2r_{\min}^2), & \text{for } \nu=0,\\[2ex] \dfrac{2}{\pi^2}\dfrac{1-r_{\min}^2}{\nu^2}, & \text{otherwise.}\end{cases} \quad (64)$$

These expressions enable us to evaluate Eq. (63). For the $\nu=0$ term in Eq. (63) we obtain 5/18. The remaining terms are evaluated within a stationary phase approximation [46]. Dropping terms with $|\nu|\geqslant 2$ we obtain

$$C^{\mathrm{cl}}(L)\sim\frac{5}{18}+\sqrt{2}\frac{16}{\pi^5}\frac{1}{\sqrt{L}}\cos\left(\pi L+\frac{\pi}{4}\right). \quad (65)$$

This result is shown in Fig. 15 together with the numerical evaluation of Eq. (61). Equation (65) proves, moreover, that the classical correlation function decays according to $\sim 1/\sqrt{L}$ for large L. This very slow decay is in fact generic for two-dimensional integrable systems. In d dimensions one obtains $\sim L^{-(d-1)/2}$. This decay is universally valid for integrable

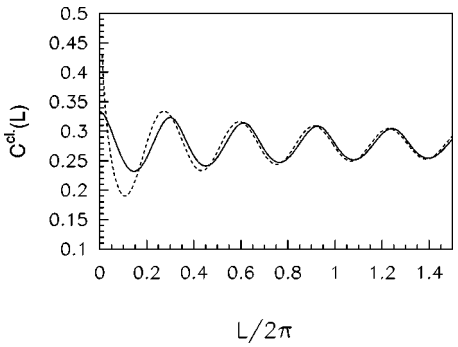

FIG. 15. Classical autocorrelation function (solid line) for $A=\boldsymbol{r}^2$, and the estimate (65) (dashed line).

systems provided the points of stationary phase are isolated and sufficiently far away from the boundary.

We conclude by briefly discussing the $t\to\infty$ limit of autocorrelations in integrable systems in comparison with the chaotic case. It is clear from Eq. (63) that in integrable systems $\langle A(t)\,A(0)\rangle\to\int d\boldsymbol{I}\,\delta[E-H(\boldsymbol{I})]\,A_0(\boldsymbol{I})^2$, where $A_0(\boldsymbol{I})$ denotes the average of the observable $A(\boldsymbol{I},\boldsymbol{\theta})$ over the torus with actions $\boldsymbol{I}$. In chaotic systems, on the other hand, $\langle A(t)\,A(0)\rangle\to\langle A\rangle^2$ for large t. Assuming that the phase space average $\langle A\rangle$ vanishes, autocorrelations in chaotic systems decorrelate for large times. In general this is not true in integrable systems, where autocorrelations decay to a variance of torus averages.

2. Weyl contributions: general case

In the preceding section, the Weyl contribution to $C(z,L)$ was analyzed. We observed oscillatory behavior as a function of L, with an envelope decaying according to $\sim L^{-(d-1)/2}$ in d dimensions. This behavior is shown in Fig. 15. An analytical estimate for the envelope of $\langle C(z,L)\rangle$ was given for large L. In the present section we focus on the oscillations in $\langle C(z,\Delta z)\rangle$ as shown in Figs. 14 and 15. The oscillatory structure is most conveniently analyzed by Fourier transformation with respect to Δz.

We first consider the rotationally invariant case, using $A=\boldsymbol{r}^2$. Using Eq. (42) we have in scaled variables

$$\langle C(z,\Delta z)\rangle=\langle d(z)\rangle\Bigg[\,\delta(\Delta z)\,\frac{4}{\pi}\times\int_0^1 dr_{\min}\,\sqrt{1-r_{\min}^2}\,\tfrac{1}{9}\,(1+2r_{\min}^2)^2+\sum_{\nu_2\neq 0}\frac{4}{\pi}\int_0^1 dr_{\min}\,\sqrt{1-r_{\min}^2}\left(\frac{2}{\pi}\,\frac{1-r_{\min}^2}{\nu_2^2}\right)^2\times\delta(F_{\nu_2}(\Delta z,r_{\min}))\Bigg] \tag{66}$$

with $F_{\nu_2}(\Delta z,r_{\min})=\Delta z-\nu_2\pi/\sqrt{1-r_{\min}^2}$. Individual terms in the sum over ν_2 will contribute whenever $F_{\nu_2}(\Delta z,r_{\min})=0$. The contribution at these points is weighted by the inverse of $|\partial F_{\nu_2}/\partial r_{\min}|$. Whenever $\partial F_{\nu_2}/\partial r_{\min}=0$, the function $\langle C(z,\Delta z)\rangle$ will hence exhibit a resonance. Figure 16 (bottom) shows the solutions of $F_{\nu_2}(\Delta z,r_{\min})=0$ for $\nu_2=1$, 2, and 3. The corresponding resonance structure,

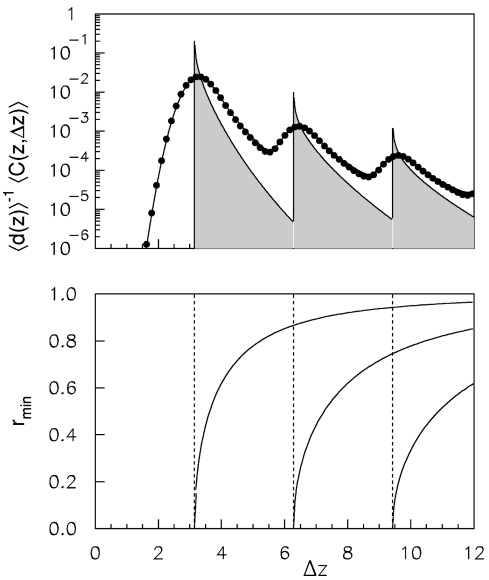

FIG. 16. (bottom) Solutions of $F_{\nu_2}(\Delta z,r_{\min})=0$. Δz is plotted as a function of $r_{\min}$ for $\nu_2=1$, 2 and 3. The dashed lines show the position of the resonances. (top) Quantum-mechanical data (●) for $\langle d(z)\rangle^{-1}\langle C(z,\Delta z)\rangle$ for the operator $A=\boldsymbol{r}^2$, together with the semiclassical estimate (solid line), a smoothed version of Eq. (67). Also shown is the unsmoothed resonance spectrum (shaded) according to Eq. (67).

$$\langle C(z,\Delta z)\rangle=\langle d(z)\rangle\Bigg[\,\delta(\Delta z)\,\frac{5}{18}+\frac{16}{\pi^5}\sum_{\nu_2=1}^{[\Delta z/\pi]}\frac{1}{\nu_2^5}\,\frac{(\nu_2\pi/\Delta z)^{12}}{\sqrt{1-(\nu_2\pi/\Delta z)^2}}, \tag{67}$$

is shown in Fig. 16 (top). Also shown are quantum-mechanical data for $\langle C(z,\Delta z)\rangle$ together with a smoothed version of Eq. (67). In all cases, the diagonal contribution giving rise to the singular part of Eq. (67) has been subtracted. We observe excellent agreement.

In the remainder of this section we discuss dipolar operators, such as $A=x$. Generalization to more general operators such as, for instance, $A=xf(|\boldsymbol{r}|)$ for a smooth but otherwise arbitrary function f is straightforward. For $A=x$ one obtains in scaled variables

$$\langle C(z,\Delta z)\rangle=\langle d(z)\rangle\sum_{\nu_1=\pm 1}\sum_{\nu_2\neq 0}\frac{4}{\pi}\times\int_0^1 dr_{\min}\,\sqrt{1-r_{\min}^2}\,|x_{\boldsymbol{\nu}}(r_{\min})|^2\,\delta[F_{\boldsymbol{\nu}}(\Delta z,r_{\min})]\,, \tag{68}$$

with $F_{\boldsymbol{\nu}}(\Delta z,r_{\min})=\Delta z+\nu_1(\arccos(r_{\min})+\nu_2\pi)/\sqrt{1-r_{\min}^2}$. Figure 17(a) shows $\langle C(z,\Delta z)\rangle$ as a function of Δz as calculated from Eq. (68). In order to allow for comparison with quantum-mechanical calculations, a finite broadening ϵ was introduced in Eq. (68). Also shown are results of a quantum

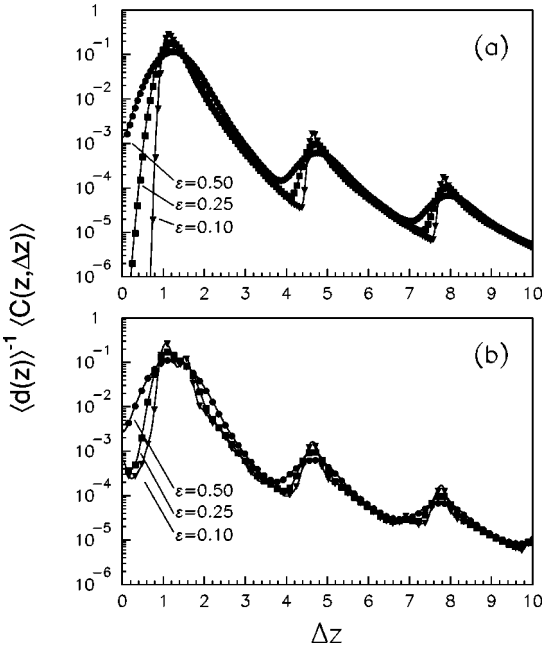

FIG. 17. (a) Quantum-mechanical data for $\langle d(z)\rangle^{-1}\langle C(z,\Delta z)\rangle$ for the operator $A=x$, together with the results from Eq. (68). (b) the same, but for the chaotic case ($a=1/2$).

mechanical calculation, for the same values of ϵ (Gaussian smoothing). The quantum and classical results agree very well with each other. Figure 17(b) shows the corresponding data for the chaotic case. We observe that the resonances in Fig. 17(a) are sharper as compared with those in Fig. 17(b). This is a consequence of the symmetries of the integrable system enforcing selection rules.

3. Periodic orbits

In the present section we turn to the oscillatory contributions to $C(z,\Delta z)$. According to Eq. (57), the oscillatory contributions are given as a sum over rational tori $\boldsymbol{M}$. The semiclassical amplitudes are weighted with torus averages of autocorrelations (40) or (59).

We evaluate Eq. (59) for two cases: for rotationally invariant and for dipolar operators. To begin with, consider the observable $A=\boldsymbol{r}^2$ which is rotationally invariant. In scaled variables we have $C_{\boldsymbol{M}}(L)=\frac{1}{6}[1-L^2(L-2\sin(\pi\nu_{\boldsymbol{M}})^2]+\frac{1}{15}[1+4\cos^2(\pi M_1/M_2)]^2$. Due to the high symmetry of the integrable problem, $C_{\boldsymbol{M}}(L)$ is periodic in $L_{\boldsymbol{M}}/M_2$. Given the analytical expression for $C_{\boldsymbol{M}}(L)$ we are in a position to assess the periodic-orbit contents of Eq. (57). Since the first term in Eq. (57) is only the leading-order approximation to the mean density, we extract $\langle C(z,\Delta z)\rangle$ numerically and subtract it. In order to extract the length spectrum of $C(z,\Delta z)$ we compute the double Fourier transformation of $z^{-1/2}C(z,\Delta z)$ with respect to z and Δz. The conjugate lengths are ΔL and L, respectively, as in Sec. V A. The amplitudes are modulated by the autocorrelation functions $C_{\boldsymbol{M}}(L)$ as shown in Fig. 18. The overall agreement between the quantum-mechanical amplitudes and the analytical estimate (57) is satisfactory. We note that for tori with $M_1=1$ and large M_2 (whispering gallery tori), the autocorrelation functions tend to $C_{\boldsymbol{M}}(L)\sim 1$, the average of $A=\boldsymbol{r}^2$ along the unit circle.

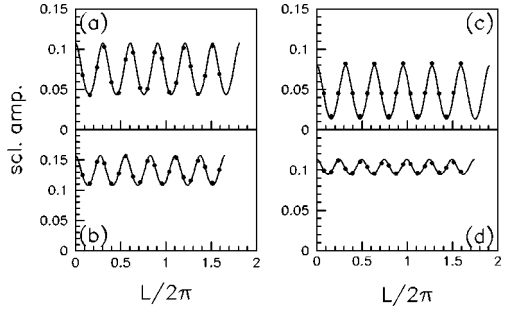

FIG. 18. Periodic orbit contributions to $C(z,\Delta z)$ for $A=\boldsymbol{r}^2$. (a) shows the semiclassical amplitude for the torus $\boldsymbol{M}=(2,5)$ calculated analytically from Eqs. (57) (solid line) and extracted from $C(z,\Delta z)$ (solid dots). (b) shows the same, but for $\boldsymbol{M}=(1,3)$, (c) for $\boldsymbol{M}=(1,2)$, and (d) for $\boldsymbol{M}=(2,7)$.

Figure 19 shows the quantum-mechanical and semiclassical amplitudes for two cases. First, the top curve in Fig. 19 shows the amplitudes for the torus $\boldsymbol{M}=(2,5)$ for the integrable case. Second, the two lower curves show the amplitudes for two star-shaped orbits in the nonintegrable case ($a=1/2$). As the value of a is increased from zero, the rational torus $\boldsymbol{M}=(2,5)$ breaks up into isolated periodic orbits. At $a=1/2$, we find that the two star-shaped orbits are both unstable. We observe that the integrable case exhibits high-symmetry (periodicity with $L_{\boldsymbol{M}}/M_2$). In the case of broken symmetry ($a=1/2$), the distance between subsequent hits on the boundary is no longer constant (or, equivalently, the integrals of motion $\boldsymbol{I}$ are destroyed) and the period of the autocorrelation functions is given by the full length L_p of the respective orbit.

We conclude this section by briefly discussing the dipole operator $A=x$. In this case, the autocorrelation function (40) modulating the semiclassical amplitudes cannot be calculated analytically. We will therefore start from Eq. (43). The coefficients $A_{\boldsymbol{\nu}}(\boldsymbol{I}_{\boldsymbol{M}})$ can be calculated numerically, as well as the summation over $\boldsymbol{\nu}$. The results are shown in Fig. 20, for several different tori $\boldsymbol{M}$, as a function of scaled frequency Δz. We also show the results of an exact quantum calculation. The quantum amplitudes are extracted from the quantum data by Fourier transform with respect to z, as described above. We observe excellent agreement between the quantum calculations and the semiclassical theory.

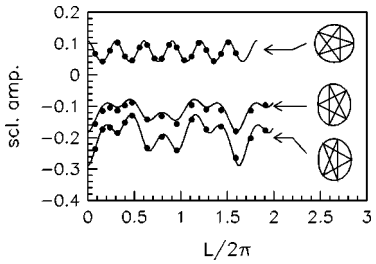

FIG. 19. Comparison of semiclassical amplitudes for the integrable and the chaotic case. The uppermost curve shows the semiclassical amplitude for the integrable system ($a=0$) corresponding to the torus $\boldsymbol{M}=(2,5)$. The two lower curves show semiclassical amplitudes for the chaotic case ($a=1/2$) corresponding to the two orbits shown in the figure. Compare Figs. 2.

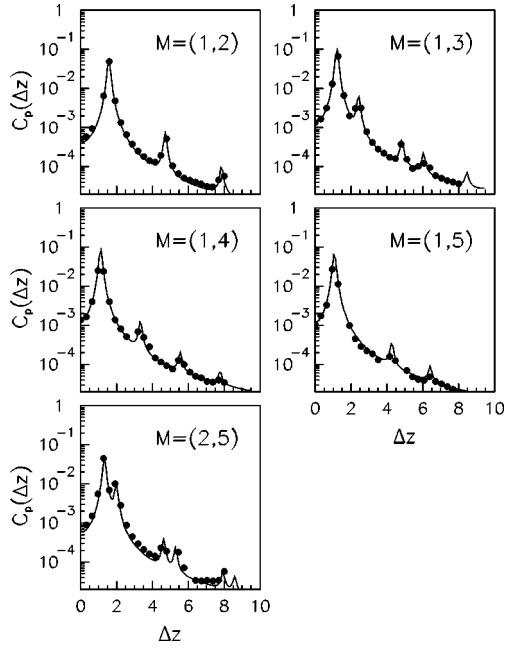

FIG. 20. Shows a comparison between the amplitudes $C_p(\Delta z)$ extracted from the quantum-mechanical data for $A=x$ (in the integrable case) compared with their semiclassical approximations; for the tori $\boldsymbol{M}=(1,2)$, $\boldsymbol{M}=(1,3)$, $\boldsymbol{M}=(1,4)$, $\boldsymbol{M}=(1,5)$, and $\boldsymbol{M}=(2,5)$. The quantum data are shown as ●, the semiclassical theory as solid lines.

VI. RESPONSE FUNCTIONS

In the two previous sections we described the semiclassical analysis of Eq. (6) according to the theory laid out in Sec. III. We have shown that the structures in $C(E,\hbar\omega)$ closely reflect the way in which classical phase space is organized. We have described the influence of phase space inhomogeneities in chaotic, ergodic systems and have discussed regular systems, where phase space is organized as a foliation of tori.

In this section we wish to point out that the function $C(E,\hbar\omega)$ is also of considerable interest experimentally since it governs the response of the quantum system in question to external perturbations. This is immediately obvious since the response of a quantum system is given by the transition amplitudes according to Fermi's golden rule. To be more precise, we note that the response of a quantum system to an external, time-dependent perturbation is given by

$$\chi(\mu,\omega)=\frac{1}{i\hbar}\int_0^\infty dt\,\langle[\hat{A}_t,A]_-\rangle\exp(i\omega t) \tag{69}$$

where $\hat{A}_t=\exp(-i\hat{H}t/\hbar)\hat{A}\exp(i\hat{H}t/\hbar)$ and $\hat{A}$ does not commute with the Hamiltonian $\hat{H}$. In terms of eigenenergies E_α and eigenstates ψ_α of $\hat{H}$, one has

$$\chi(\mu,\omega)=\sum_{\alpha,\beta}\frac{f_\alpha-f_\beta}{\hbar\omega-E_\alpha+E_\beta+i\eta}\langle\psi_\alpha|\hat{A}|\psi_\beta\rangle\langle\psi_\beta|\hat{A}|\psi_\alpha\rangle, \tag{70}$$

where $f_\alpha=f(E_\alpha)=[\exp(\beta(E_\alpha-\mu)+1]^{-1}$ is the Fermi function, $\beta=(k_BT)^{-1}$ and μ is the chemical potential. For the imaginary part of χ we have

$$\chi''(\mu,\omega)=-\pi\int dE\,[f(E)-f(E-\hbar\omega)]\sum_{\alpha,\beta}\langle\psi_\alpha|\hat{A}|\psi_\beta\rangle \times\langle\psi_\beta|\hat{A}|\psi_\alpha\rangle\,\delta(\hbar\omega-E_\alpha+E_\beta)\,\delta(E-E_\alpha). \tag{71}$$

Assuming that both $\hbar\omega$ and β^{-1} are small compared to energy scales over which the integrand differs significantly from its value at μ, we expand $f(E-\hbar\omega)\simeq f(E)-f'(E)\hbar\omega$. This gives

$$\chi''(\mu,\omega)=-\pi\hbar\omega\int dE\,f'(E)\sum_{\alpha,\beta}\langle\psi_\alpha|\hat{A}|\psi_\beta\rangle \times\langle\psi_\beta|\hat{A}|\psi_\alpha\rangle\,\delta(\hbar\omega-E_\alpha+E_\beta)\,\delta(E-E_\alpha). \tag{72}$$

Making use of the expressions derived in Sec. III, one obtains

$$\chi''(\mu,\omega)=-\pi\hbar\omega\int dE\,f'(E) \times\int_{-\infty}^{\infty}dt\,e^{i\omega t}\langle A(\boldsymbol{p}_t,\boldsymbol{r}_t)A(\boldsymbol{p},\boldsymbol{r})\rangle. \tag{73}$$

Equation (73) is the desired classical approximation to $\chi''(\mu,\omega)$. We emphasize that in the derivation it has been assumed that the Fourier transform of $\langle A(\boldsymbol{p}_t,\boldsymbol{r}_t)A(\boldsymbol{p},\boldsymbol{r})\rangle$ with respect to t varies sufficiently slowly on the scale of $\hbar\omega$ and β^{-1}.

The real part $\chi'(\mu,\omega)$ of the susceptibility can be obtained along similar lines. In the following, however, we give a slightly different derivation that leads to a form clearly exhibiting the symmetry properties of the classical approximation to $\chi(\mu,\omega)$. We start from Eq. (69) and approximate the commutator by the Poisson bracket $[,]\simeq-i\hbar\{,\}$. This is analogous to the approximation (14). One obtains

$$\chi(\mu,\omega)=\int_0^\infty dt e^{i\omega t}\int d\boldsymbol{p}d\boldsymbol{r}\;f'[H(\boldsymbol{p},\boldsymbol{r})] \times\{A(\boldsymbol{p}_t,\boldsymbol{r}_t),H(\boldsymbol{p},\boldsymbol{r})\}\,A(\boldsymbol{p},\boldsymbol{r}),$$

assuming that the boundary terms vanish. Using the classical equations of motion we obtain

$$\chi(\mu,\omega)=\int_0^\infty dt\exp(i\omega t) \times\int dEf'(E)\frac{d}{dt}\langle A(\boldsymbol{p}_t,\boldsymbol{r}_t)A(\boldsymbol{p},\boldsymbol{r})\rangle. \tag{74}$$

We introduce the classical function

$$I(\mu,\omega)=-\frac{1}{2\pi}\int_{-\infty}^{\infty}dt\;e^{i\omega t}\int dEf'(E)\langle A(\boldsymbol{p}_t,\boldsymbol{r}_t)A(\boldsymbol{p},\boldsymbol{r})\rangle =-\int dE\,f'(E)C(E,\omega). \tag{75}$$

At low temperatures, $T \to 0$, we have $I(\mu,\omega) \to C(E,\omega)$. Using Eq. (74) we obtain the following representation for the susceptibility

$$\chi(\mu,\omega) = -\int_{-\infty}^{\infty} d\omega' \frac{\omega' I(\mu,\omega')}{\omega - \omega'}. \tag{76}$$

For the real and imaginary parts of the susceptibility we obtain

$$\chi'(\mu,\omega) = \mathcal{P}\int_{-\infty}^{\infty} d\omega' \frac{\omega' I(\mu,\omega')}{\omega - \omega'},$$

$$\chi''(\mu,\omega) = -\pi\omega I(\mu,\omega). \tag{77}$$

The second of Eqs. (77) is just Eq. (73). These equations constitute a classical approximation for the real and imaginary parts of $\chi(\mu,\omega)$. Equations (77) are of the same form as the spectral representation for susceptibilities in quantum mechanics. The quantum spectral function is replaced by a classical spectral function $I(\mu,\omega)$.

For integrable systems, an explicit expression for $I(\mu,\omega)$ can be derived as follows. Using Eqs. (38) and (41), we obtain

$$I(\mu,\omega) = -\int d\boldsymbol{I} f'[H(\boldsymbol{I})] \times \sum_{\boldsymbol{\nu}} A^*_{\boldsymbol{\nu}}(\boldsymbol{I}) A_{\boldsymbol{\nu}}(\boldsymbol{I})\, \delta[\omega - \boldsymbol{\nu}\cdot\boldsymbol{\omega}(\boldsymbol{I})]. \tag{78}$$

Substituting this into Eq. (76), we obtain

$$\chi(\mu,\omega) = \int d\boldsymbol{I} f'[H(\boldsymbol{I})] \times \sum_{\boldsymbol{\nu}} A^*_{\boldsymbol{\nu}}(\boldsymbol{I}) A_{\boldsymbol{\nu}}(\boldsymbol{I}) \frac{\boldsymbol{\nu}\cdot\boldsymbol{\omega}(\boldsymbol{I})}{\omega - \boldsymbol{\nu}\cdot\boldsymbol{\omega}(\boldsymbol{I}) + i0^+}. \tag{79}$$

This provides an easily evaluated classical approximation for susceptibilites in classically integrable quantum systems, in terms of the Fourier coefficients of the observable $A(\boldsymbol{I},\boldsymbol{\theta})$, which are periodic functions of $\boldsymbol{\theta}$ on a given torus $\boldsymbol{I}$, and in terms of the corresponding frequencies $\boldsymbol{\nu}\cdot\boldsymbol{\omega}$.

For chaotic systems, there is no explicit expression available for $I(\mu,\omega)$ — such as Eq. (78) for integrable systems. In ergodic systems, however, the phase-space average in Eq. (73) can be evaluated as a time average along an ergodic trajectory.

Equations (77) show that the resonance structures discussed in Secs. V A 2 and V A 3 can, in principle, be found experimentally. In Refs. [26,27,46] a possible absorption experiment was discussed where these structures would be relevant. We note that our semiclassical treatment allows us to justify and extend the classical model of the static magnetocoductivity in antidot arrays discussed in Ref. [25]. We reproduce the classical model for the magnetoconductivity from Eqs. (6) where $\omega = 0$ and $A = j_x$ (j_x is the current in x direction),

$$\sigma_{xx}(E_{\mathrm{F}}) = \omega^{-1}\chi''(E_{\mathrm{F}},\omega=0)\,. \tag{80}$$

The antidot arrays studied experimentally [48] exhibit mixed classical dynamics, where stable islands coexist with connected chaotic regions in phase space. Our theory can be extended to this case in the following way. We group our states into those associated with stable islands (regular states) and irregular states associated with the chaotic phase-space regions [49,50]. We neglect nondiagonal matrix elements between regular and irregular states (assuming that they are exponentially suppressed). Then Eq. (6) consists of two terms,

$$C(E,\hbar\omega) \simeq C^{\mathrm{reg}}(E,\hbar\omega) + C^{\mathrm{irreg}}(E,\hbar\omega)\,. \tag{81}$$

$C^{\mathrm{irreg}}(E,\hbar\omega)$ can be analyzed according to the semiclassical formulas set out in Sec. III A, and $C^{\mathrm{reg}}(E,\hbar\omega)$ can be calculated according to the formulas given in Sec. III B by defining action and angle variables local to a given stable island. A first step in this direction has been discussed in [28]. We note that stable islands contribute in two ways to $C(E,\hbar\omega)$. First, there is the obvious contribution through $C^{\mathrm{reg}}(E,\hbar\omega)$. Second, a stable island is surrounded by comparatively stable regions within the connected chaotic component. These comparatively stable regions cause resonances in $C^{\mathrm{irreg}}(E,\hbar\omega)$, of the nature discussed in Secs. V A 2 and V A 3.

It is clear from the discussion in Sec. III that there may be semiclassical corrections to the classical magnetoconductivity calculated in Ref. [25]. These would be of oscillatory nature and of the forms (38) or (59), for integrable and chaotic systems, respectively. Such oscillatory contributions have in fact been observed [30] and have been discussed in Refs. [31,32]. A comparison of such contributions with exact quantum-mechanical calculations was first performed in [24] and [23].

VII. SUMMARY AND CONCLUSIONS

In this article, we have reported on semiclassical sum rules constraining local densities of matrix elements in single-particle quantum systems. It was to be expected and has been worked out in detail that the semiclassical estimates depend on the nature of the dynamics of the classical system. We have studied systems exhibiting chaotic, largely ergodic dynamics and systems with regular classical dynamics.

In both cases, there are two contributions to the sum rules: a smooth and an oscillatory part. The smooth contribution is given as the Fourier transform of a classical correlation function. This is of course true in both cases, for ergodic and for regular systems. In ergodic systems, this correlation function may be evaluated along an ergodic trajectory. Despite being ergodic, however, the energy shell may be far from homogeneous. The ergodic trajectory may be trapped in the vicinity of weakly unstable regions. We have shown how this intermittent behavior gives rise to pronounced resonances in the smooth part of the quantum density. Quantum mechanically, these resonances are due to wave function localization in the vicinity of weakly unstable regions in phase space. Classically, these structures are just resonances in the autocorrelation function. We have discussed this analogy and analyzed it quantitatively.

In regular systems, the smooth contribution is also given as a phase-space average of autocorrelations. In this case, however, the invariant objects in phase space are tori and we

average over autocorrelations on tori in order to obtain the smooth contribution to the quantum density of nondiagonal matrix elements. There are three important differences from the ergodic case. First, the resonances are sharper in integrable systems. This is a consequence of selection rules due to the high symmetry of integrable systems. Second, motion along invariant tori is always (quasi)periodic and thus decorrelates very slowly. As a function of t — the variable conjugate to the energy separation $\hbar\omega = E_\alpha - E_\beta$ between initial and final states — the smooth contribution decays as $\sim t^{-(d-1)/2}$ for large t. This was shown within a stationary phase analysis and is valid provided the points of stationary phase are isolated and sufficiently far away from the boundary. Third, in ergodic systems $\langle C(E,t)\rangle$ has the following limiting behavior for large times: $\langle C(E,t)\rangle \sim \langle d(E)\rangle \langle A\rangle^2$. In integrable systems, on the other hand, one finds $\langle C(E,t)\rangle \sim \langle d(E)\rangle \int d\boldsymbol{I}\, \delta[E - H(\boldsymbol{I})]\, A_0(\boldsymbol{I})^2$, where $A_0(\boldsymbol{I})$ denotes the average of the observable $A(\boldsymbol{I},\boldsymbol{\theta})$ over the torus with actions $\boldsymbol{I}$.

In addition to the smooth part, semiclassical theory predicts periodic orbit contributions to the quantum densities. We have analyzed the periodic orbit contributions in detail, for integrable as well as for chaotic systems. Again, the similarity between the integrable and the chaotic is apparent: exploiting the scaling property of the system, the contribution of each orbit may be obtained by Fourier transformation of the oscillating part of the spectral function with respect to a scaled energy variable. In the chaotic case, we find the amplitudes to be modulated by correlation functions along the respective isolated periodic orbits. In the integrable case, these amplitudes are averaged over all periodic orbits on a given torus.

In summary, we have provided a comprehensive and conclusive study of all aspects of the semiclassical evaluation of local densities of quantum-mechanical matrix elements. This includes, in particular, the results of two previously published articles [24,23] and goes considerably beyond what could be discussed there.

The results published in this paper are not only of interest theoretically. As we have pointed out, the density of nondiagonal matrix elements characterizes the linear response of quantum systems to external, time-dependent perturbations. Using the framework provided in this article, it is possible to derive classical and semiclassical approximations to quantum-mechanical response functions. Most recently, using the results of this article, we have studied the response of small metal particles to electromagnetic radiation, for diffusive [29] and for ballistic dynamics [47], and taking into account the magnetic dipole interaction in both diffusive and ballistic systems [51].

ACKNOWLEDGMENTS

This work was supported in part by the SFB 393 (Chemnitz).

APPENDIX: SEMICLASSICAL QUANTIZATION FOR SCALING SYSTEMS

In this Appendix we summarize, for convenience, several well-known facts about scaling systems. In a scaling system, the Hamiltonian phase flow may be parameterized such that all quantities characterizing classical motion are energy independent. In a billiard with $m = 1/2$, for example, solutions of Hamilton's equations at energies E and $E_0 = 1$ are related via the transformation

$$\boldsymbol{p}(t) = \sqrt{E}\,\boldsymbol{p}_0(t_0), \quad \boldsymbol{r}(t) = \boldsymbol{r}_0(t_0), \tag{A1}$$

provided the time t is scaled appropriately, $t = E^{-1/2} t_0$. Other observables are assumed to scale as

$$A(\boldsymbol{p},\boldsymbol{r}) = E^{\gamma} A_0(\boldsymbol{p}_0,\boldsymbol{r}_0) \tag{A2}$$

which defines the exponent γ. The Maupertuis action along a trajectory scales as

$$S = \int \boldsymbol{p}\, d\boldsymbol{r} = \sqrt{E} \int \boldsymbol{p}_0\, d\boldsymbol{r}_0 \equiv z S_0 \tag{A3}$$

with $z = \sqrt{E}$. One notes that the scaled action $S_0 = \int \boldsymbol{p}_0 d\boldsymbol{q}_0$ is just the arclength L along the trajectory, since $S_0 = \partial S/\partial z = t\,\partial E/\partial z = 2zt = L$. The phase flow in L is generated by $\sqrt{H(\boldsymbol{p},\boldsymbol{r})}$.

There is no direct analogue in quantum mechanics, since the quantum-mechanical propagator corresponding to $\sqrt{H(\boldsymbol{p},\boldsymbol{r})}$ does not satisfy Schrödinger's equation. As is well known, however, a scaled version of Gutzwiller's trace formula may be obtained by defining $d(z)\, dz = d(E)\, dE$. Starting from Eq. (49) one has with $T_p = \partial S_p/\partial E$ and $z_\alpha = E_\alpha^{1/2}$,

$$d_A(z) \equiv \sum_\alpha \langle \psi_\alpha | \hat{A} | \psi_\alpha \rangle\, \delta(z - z_\alpha) = \langle d_A(z)\rangle + \frac{1}{\pi} \mathrm{Re} \sum_{p,r} L_p\, w_{pr}\, A_p \exp[r(izL_p - i\pi\mu_p/2)]. \tag{A4}$$

Equation (A4) is a Fourier series in z and the contribution of each periodic orbit to the density of states may be easily extracted by Fourier transformation [52]. In order to eliminate all energy dependences of the semiclassical amplitudes, the operators should be scaled with energy according to their classical scaling properties (A2).

To derive a scaling expression for non-diagonal matrix elements, one makes use of the following scaling relation for

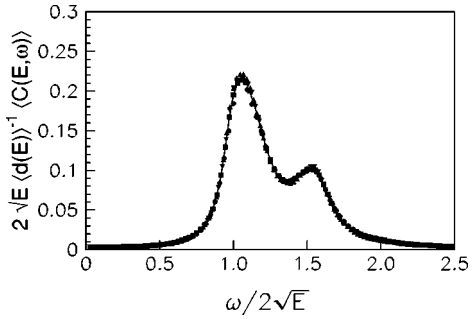

FIG. 21. Scaling behavior of the spectral function $C(E,\omega)$ for $A = x$ and $\eta = 0.2$. Shown are various values of $z = \sqrt{E}$, namely $z = 80$ (●), $z = 90$ (■), $z = 100$, and $z = 110$.

autocorrelation functions, $C(E,t)=E^{2\gamma}f(2\sqrt{E}t)=E^{2\gamma}f(L)$. Applying this to the Weyl part of $C(E,\omega)$, one obtains (with $\hbar=1$)

$$\langle C(E,\omega)\rangle = 2E^{1/2+2\gamma}\langle d(E)\rangle\, f(\omega/2\sqrt{E}). \tag{A5}$$

In Fig. 21, we show $\langle C(E,\omega)\rangle$ for $A=x$ as a function of ω for several values of E. After scaling the x and y axis appropriately, the data fall on the same energy-independent curve $f(\ )$. A similar scaling relation holds for the periodic-orbit contributions. This scaling property suggests to work from the outset with scaled variables $z=\sqrt{E}$ and $\Delta z=\omega/2\sqrt{E}$, i.e., to consider

$$C(z,\Delta z)=\sum_{\alpha\beta}\ |\langle\psi_\alpha|\hat{A}|\psi_\beta\rangle|^2\,\delta(z-z_\alpha)\,\delta(\Delta z-z_\alpha+z_\beta),$$

which has the semiclassical expansion

$$C(z,\Delta z)=\langle C(z,\Delta z)\rangle + \frac{1}{\pi}\mathrm{Re}\sum_{p,r}\ C_p(\Delta z)\,L_p\,w_{pr}\exp[r(izL_p-i\pi\mu_p/2)] \tag{A6}$$

with

$$\langle C(z,\Delta z)\rangle \simeq \langle d(z)\rangle\,\frac{1}{2\pi}\int_{-\infty}^{\infty} dL\,\exp(i\Delta z L)\,C^{\mathrm{cl}}(L)$$

and $C_p(\Delta z)$ defined analogously. Unlike Eq. (A4), the scaled sum rule (A6) is not exact. It is valid provided $z \gg \Delta z$.

[1] M. Berry, in *Chaos and Quantum Physics*, edited by M. J. Giannoni, A. Voros, and J. Zinn-Justin (North–Holland, Amsterdam, 1991), p. 251.
[2] M. Gutzwiller, *Chaos in Classical and Quantum Mechanics* (Springer, Berlin, 1990).
[3] C. E. Porter, *Statistical Theories of Spectra* (Academic, New York, 1965), p. 2.
[4] M. Wilkinson, Phys. Rev. A **41**, 4645 (1991).
[5] M. Wilkinson, J. Phys. A **21**, 1173 (1988).
[6] E. B. Bogomolny and J. P. Keating, Phys. Rev. Lett. **77**, 1472 (1996).
[7] B. Eckhardt *et al.*, Phys. Rev. E **52**, 5893 (1995).
[8] B. Eckhardt and J. Main, Phys. Rev. Lett. **75**, 2300 (1995).
[9] M. Wilkinson and P. N. Walker, J. Phys. A **28**, 6143 (1996).
[10] P. Jacquod and J.-P. Amiet, J. Phys. A **30**, 2963 (1997).
[11] B. Eckhardt, Physica D **109**, 53 (1997).
[12] A. Bäcker, R. Schubert, and P. Stifter, Phys. Rev. E **57**, 5425 (1998); **58**, 5192E (1998).
[13] T. O. de Carvalho, J. Robbins, and J. P. Keating, J. Phys. A **31**, 5631 (1998).
[14] B. Mehlig and N. Taniguchi (unpublished).
[15] M. Feingold and A. Peres, Phys. Rev. A **34**, 591 (1986).
[16] M. Wilkinson, J. Phys. A **20**, 2415 (1987).
[17] B. Eckhardt, S. Fishman, K. Müller, and D. Wintgen, Phys. Rev. A **45**, 3531 (1992).
[18] E. J. Austin and M. Wilkinson, Europhys. Lett. **20**, 589 (1992).
[19] E. J. Austin and M. Wilkinson, Nonlinearity **5**, 1137 (1992).
[20] T. Prosen and M. Robnik, J. Phys. A **26**, 319 (1993).
[21] T. Prosen, Ann. Phys. (N.Y.) **27**, 115 (1994).
[22] D. Boosé, J. Main, B. Mehlig, and K. Müller, Europhys. Lett. **32**, 295 (1995).
[23] B. Mehlig, Phys. Rev. B **55**, 10 193 (1997).
[24] B. Mehlig, D. Boosé, and K. Müller, Phys. Rev. Lett. **75**, 57 (1995).
[25] R. Fleischmann, T. Geisel, and R. Ketzmerick, Phys. Rev. Lett. **68**, 1367 (1992).
[26] D. Weiss, G. Leutjering, and K. Richter, Chaos Solitons Fractals **8**, 1337 (1997).
[27] E. J. Austin and M. Wilkinson, J. Phys.: Condens. Matter **5**, 8461 (1993).
[28] M. Wilkinson and E. J. Austin, J. Phys.: Condens. Matter **6**, 4153 (1994).
[29] B. Mehlig and M. Wilkinson, J. Phys.: Condens. Matter **9**, 3277 (1997).
[30] D. Weiss *et al.*, Phys. Rev. Lett. **70**, 4118 (1993).
[31] K. Richter, Europhys. Lett. **29**, 7 (1995).
[32] G. Hackenbroich and F. v. Oppen, Z. Phys. B **97**, 157 (1995).
[33] M. Robnik, J. Phys. A **16**, 3971 (1983).
[34] M. Robnik, J. Phys. A **17**, 1049 (1983).
[35] T. Prosen, J. Phys. A **27**, 569 (1994).
[36] J. B. Keller and S. I. Rubinow, Ann. Phys. (N.Y.) **9**, 24 (1960).
[37] A. Hayli, T. Dumont, J. Moulin-Ollagnier, and J.-M. Strelcyn, J. Phys. A **20**, 3237 (1987).
[38] M. Berry, Philos. Trans. R. Soc. London, Ser. A **287**, 30 (1977).
[39] M. V. Berry and M. Tabor, J. Phys. A **10**, 371 (1977).
[40] M. V. Berry and M. Tabor, Proc. R. Soc. London, Ser. A **349**, 101 (1977).
[41] M. Kac, Am. Math. Monthly **73**, 1 (1966).
[42] I. Ussishkin, Master's thesis, Feinberg Graduate School, Weizmann Institute of Science, 1994.
[43] B. Eckhardt, J. M. G. Llorente, and E. Pollak, Chem. Phys. Lett. **174**, 325 (1990).
[44] The coordinate system on the surface of section is then not canonical, but this is irrelevant for the present purpose.
[45] K. Müller and D. Wintgen, J. Phys. B **27**, 2693 (1994).
[46] G. Casati, F. Valzgris, and I. Guarneri, Physica D **3**, 644 (1981).
[47] B. Mehlig and K. Richter, Phys. Rev. Lett. **80**, 1936 (1998).
[48] D. Weiss *et al.*, Phys. Rev. Lett. **66**, 2790 (1991).
[49] I. C. Percival, J. Phys. B **6**, 229 (1973).
[50] I. C. Percival, Adv. Chem. Phys. **36**, 1 (1977).
[51] M. Wilkinson, B. Mehlig, and P. Walker, J. Phys. C **10**, 2739 (1998).
[52] D. Wintgen, Phys. Rev. Lett. **58**, 1589 (1987).